Cytosolic aspartate aminotransferase moonlights as a ribosome binding modulator of Gcn2 activity during oxidative stress

Robert A. Crawford[1], Mark P. Ashe[1], Simon J. Hubbard[2] and Graham D. Pavitt[1]*

Email addresses	ORCID numbers
robert.crawford@manchester.ac.uk	0000-0002-9788-5137
mark.p.ashe@manchester.ac.uk	0000-0002-4457-7851
simon.hubbard@manchester.ac.uk	0000-0002-8601-9524
graham.pavitt@manchester.ac.uk	0000-0002-8593-2418

*Correspondence to GDP

[1]Division of Molecular and Cellular Function, or [2]Division of Evolution, Infection and Genomics

Faculty of Biology Medicine and Health, Manchester Academic Health Science Centre, The University of Manchester, Oxford Road, Manchester, M13 9PT, UK

Abstract

Regulation of translation is a fundamental facet of the cellular response to rapidly changing external conditions. Specific RNA-binding proteins (RBPs) co-ordinate the translational regulation of distinct mRNA cohorts during stress. To identify RBPs with previously under-appreciated roles in translational control, we used polysome profiling and mass spectrometry to identify and quantify proteins associated with translating ribosomes in unstressed yeast cells and during oxidative stress and amino acid starvation, which both induce the integrated stress response (ISR). Over 800 proteins were identified across polysome gradient fractions, including ribosomal proteins, translation factors and many others without previously described translation-related roles, including numerous metabolic enzymes. We identified variations in patterns of polysome enrichment in both unstressed and stressed cells and identified proteins enriched in heavy polysomes during stress. Genetic screening of polysome-enriched RBPs identified the cytosolic aspartate aminotransferase, Aat2, as a ribosome-associated protein whose deletion conferred growth sensitivity to oxidative stress. Loss of Aat2 caused aberrantly high activation of the ISR via enhanced eIF2α phosphorylation and *GCN4* activation. Importantly, non-catalytic *AAT2* mutants retained polysome association and did not show heightened stress sensitivity. Aat2 therefore has a separate ribosome-associated translational regulatory or 'moonlighting' function that modulates the ISR independent of its aspartate aminotransferase activity.

Introduction

Translation and its regulation are highly complex processes requiring the concerted action of numerous factors associated with mRNAs: translation factors, tRNAs, ribosomes and RNA-binding proteins (RBPs) (Dever et al. 2016). Importantly, the translation apparatus is nimble in that its regulation immediately impacts upon the protein content of cells to meet changing conditions. Both general and mRNA-specific translational regulatory mechanisms coordinate cellular responses to diverse cues (Jackson et al. 2010). One translational control pathway common to all eukaryotes is called the integrated stress response (ISR) (Pakos-Zebrucka et al. 2016), also known as general amino acid control in yeast. Distinct cellular stress signals activate one or more of a family of protein kinases (GCN2, PKR, PERK and HRI) that each phosphorylate the general translation initiation factor eIF2 on a conserved single serine residue of its alpha subunit (Wek 2018). This causes a rapid global downregulation of protein synthesis. Under active translation conditions, eIF2 in its GTP-bound form recruits initiator tRNA to ribosomes. Phosphorylated eIF2 instead forms an inhibited complex with the key guanine nucleotide exchange factor eIF2B, which otherwise generates active eIF2-GTP (Pavitt 2018; Adomavicius et al. 2019; Kashiwagi et al. 2019). However, not all translation is inhibited by the ISR. mRNAs encoding stress-protective proteins need to be translated for cells to adapt to the altered cellular environment. The 5' untranslated regions (5'UTRs) of some translationally-controlled mRNAs contain *cis*-acting elements promoting their translation when bulk protein synthesis is attenuated (Hinnebusch et al. 2016; Wek 2018). Key examples include the mammalian *ATF4* and yeast *GCN4* mRNAs, which are both transcriptional activators whose expression is controlled via regulated ribosome reinitiation at upstream open reading frames (uORFs) (Hinnebusch et al. 2016). Once the stress has been neutralised, translation patterns revert to steady state, restoring proteostasis (Crawford and Pavitt 2019). In the ISR this requires the dephosphorylation of eIF2 (Wek 2018). In humans a failure to restore proteostasis in a timely manner can contribute to a range of diseases, including cognitive disorders and cancer (Costa-Mattioli and Walter 2020).

Other stress-dependent mechanisms also operate on translation. Inhibiting RNA helicases that promote ribosome recruitment and the unwinding of secondary structures during 5'UTR scanning has been shown to reduce translation significantly (Sen et al. 2015). In yeast, both glucose starvation and heat shock stresses are accompanied by a dramatic reduction in mRNA binding by both the eIF4A and Ded1 RNA helicases (Castelli et al. 2011; Bresson et al. 2020), which contributes to very rapid translational repression, within one minute following glucose withdrawal (Ashe et al. 2000). In addition, translation elongation can be regulated through modulation of the activity of elongation factors such as eEF2, which is modified downstream of some stress signalling pathways, including oxidative stress. tRNA

availability also controls elongation rates. Local variations in codon usage and ribosomal pausing and stalling events all slow elongation (Dever and Green 2012; Schuller et al. 2017; Wu et al. 2019; Tesina et al. 2020). Stalled ribosomes lead to ribosome collisions, which can activate Gcn2 and the ISR (Wu et al. 2020; Pochopien et al. 2021; Yan and Zaher 2021) as well as ribosome-associated quality control (RQC) pathways that recycle stalled ribosomes and degrade defective mRNAs (D'Orazio and Green 2021).

Ribosomes themselves are not necessarily uniform and can vary between conditions and cell types (Slavov et al. 2015). Variation in ribosome composition can confer preferences for binding to different subsets of mRNAs. Examples include the ribosomal protein (RP) Rps26/eS26, where both high salt and raised pH reduce its incorporation into yeast ribosomes. Rps26-deficient ribosomes are proposed to preferentially translate stress-responsive mRNAs via altered Kozak sequence recognition preferences (Ferretti et al. 2017). Furthermore, some paralogous RPs, where two genes encode the same RP, have been demonstrated to have specific roles in translational regulation. For example, yeast Rpl1a/uL1 and Rpl1b show preferences for translating different sets of mRNAs, as Rpl1b-containing ribosomes promote more efficient translation of mitochondrial proteins required for respiratory growth (Segev and Gerst 2018). Mutations in RPs lead to Diamond–Blackfan Anemia and other ribosomopathies in humans, which might imply specialised roles for RP-deficient or paralog-specific ribosomes. Alternatively, reducing the abundance of active ribosomes via defects in RPs likely changes the balance of expression of mRNAs observed in different cells or tissues, potentially contributing to ribosomopathies (Mills and Green 2017).

RNA-binding proteins (RBPs) and ribosome-interacting proteins also contribute to translational control. Several RBPs have been observed to modulate the expression of sets of target mRNAs, which range from a few target transcripts to several thousand (Hogan et al. 2008). For example, the RBP CPEB is only recruited to mRNAs containing a cytoplasmic polyadenylation element and helps to modulate ribosome recruitment and translation (Richter 2007). Multiple studies have attempted to either identify mRNA targets of specific RBPs (Hogan et al. 2008) or identify new RBPs across a range of organisms, using a variety of methods (Hentze et al. 2018). Curiously, these latter studies have uncovered an unexpectedly large number of metabolic enzymes that bind RNA. Very few of these newly recognised RBPs have a defined role in RNA biology, but it has been suggested that many could have a second ‘moonlighting’ function when bound to RNA. These results highlight the possibility that undiscovered post-transcriptional regulatory networks link gene expression and intermediary metabolism (Hentze and Preiss 2010).

A model has therefore emerged of a complex interplay between mRNA-specific elements, RBPs and ribosome-associated factors that may combine to enable selected stress-responsive mRNAs to escape globally repressive regulatory mechanisms. Here we set out to

identify candidate proteins that might be involved in mRNA-specific translational regulation during stress in yeast. Oxidative stress caused by the addition of hydrogen peroxide (H_2O_2) brings about rapid translational repression via Gcn2 activation and the ISR (Shenton et al. 2006), as well as the induction of antioxidant enzymes at both the transcriptional and translational levels to ameliorate the stress (Morano et al. 2012). How these antioxidant enzymes are translated under such repressive conditions is unclear. We took an unbiased proteomics approach to determine patterns of ribosome-association across polysome gradients in actively growing cells and how these change in response to hydrogen peroxide. In parallel we assessed how cells respond to amino acid starvation caused by the addition of 3-amino-1,2,4-triazole (3-AT), a well characterised inhibitor of histidine biosynthesis (Hinnebusch 2005). Both stresses activate the yeast ISR and translation of *GCN4* (Hinnebusch ; Shenton et al. 2006) but also need to promote the expression of different stress-specific genes. We find that the changes in polysome enrichment (PE) of proteins in response to both stresses are remarkably well-correlated, with similar changes observed across both stresses for translation factors (TFs), RPs and a wide range of RBPs including metabolic enzymes. While some RBPs closely followed the PE profiles of RPs during stress by accumulating in the 80S/monosomal fraction, other proteins maintained or enhanced their association with the remaining heavy polysomes during the stress response. By screening candidate RBP knockout strains for oxidative stress phenotypes, we identified cytoplasmic aspartate amino transferase (Aat2) as a novel ribosome-interacting protein with a 'moonlighting' function. We show that Aat2 binds to 60S ribosomes and moderates Gcn2 activation in response to hydrogen peroxide. Remarkably, mutational analyses show that the stress-response role is independent of its metabolic role.

Results

Quantification of co-ordinated alterations in polysome-association of proteins during acute stress

To gain insight into mechanisms of stress responses, we set out to identify candidate proteins that might be involved in mRNA-specific translational regulation during stress as cells adapt to their changing environment. Proteins involved in translational regulation have been found associated with the translational machinery by previous mass spectrometry (MS) approaches (Fleischer et al. 2006), and by targeted studies of individual proteins which have high PE in stressed conditions (Li et al. 2004; Hirschmann et al. 2014; Kershaw et al. 2015). Proteins with mRNA-specific activation roles may retain or enhance their PE during stress. Similarly RQC factors should be ribosome-associated during stress, as both 3-AT and H_2O_2 have been associated with enhanced slowing and stalling of ribosomes which recruits the RQC machinery and activates Gcn2 (Shenton et al. 2006; Meydan and Guydosh 2020; Yan and Zaher 2021). In contrast, the rapid loss of factors from polysomes may contribute to translational repression, as observed for eIF4A during glucose starvation and heat shock (Castelli et al. 2011; Bresson et al. 2020).

We initially compared the growth and polysome profile responses of a histidine prototrophic version of the standard yeast lab strain, BY4741, under two stress conditions: acute oxidative stress induced by hydrogen peroxide (H_2O_2) and amino acid starvation induced by addition of the His3 inhibitor 3-amino-1,2,4-triazole (3-AT). Each stressor was added during exponential growth (Figure 1A), causing an interruption to cell growth which caused a loss of polysomes by 15 minutes (Figure 1B-C), in accord with prior studies (Costello et al. 2017). Growth recovered with time, showing that the cells were able to adapt to each stressor (Figure 1A). Qualitative analysis of protein migration through 15-50% sucrose gradients by SDS-PAGE indicated that the majority of proteins were restricted to the top of the gradient, but that specific proteins did migrate deep into the gradient and were retained on polysomes (Figure 1–figure supplement 1A).

We employed polysomal proteomics to identify changes in PE for ribosome-associated proteins following treatment with either H_2O_2 or 3-AT. Proteins in sucrose gradient fractions were identified and quantified using label-free MS (Aebersold and Mann 2016), from which the PE of each in unstressed and stressed conditions could be determined. To identify such proteins we grew cell cultures to logarithmic phase (A_{600} = 0.6) and added 0.45 mM H_2O_2 or 10 mM 3-AT for 15 minutes, as these treatments had equivalent impact on ribosome run-off in polysome profiles (Figure 1B-C). We used formaldehyde treatment to stabilize ribosome associated proteins in polysomes, which gave similar results to cycloheximide fixation for known polysome-associated proteins we assessed by immunoblotting (eIF4E, Puf3,

Rps3/uS3, Rpl35/uL29; Figure 1, Figure 1–figure supplement 1B-C). Each sample was fractionated into five polysome fractions (F1-F5), where F1 represents the 80S/monosome peak and F2-F5 have increasing numbers of ribosomes per mRNA, from disomes to heavy polysomes (Figure 1B). For each fraction, as well as the respective unfractionated cytoplasmic lysates (Totals, T), four biological replicates (originating from separate yeast colonies) were analysed using label-free MS (Aebersold and Mann 2016). Between 145 and 767 unique proteins were identified in at least two replicates of individual fractions (Figure 1D, Supplementary file 1–sheets 1 and 2). There was excellent correlation of the measured protein signal between replicates for unstressed fractions F1-F5 (r^2 typically >0.9), but more divergence for stressed samples, especially in F4-F5 where, as expected from global polysome profiles, fewer proteins were found migrating deep into the gradient (Figure 1–figure supplement 2A). Principal component analysis (PCA) showed good clustering of replicates for all three conditions, with adjacent sucrose gradient fractions indicating a gradual change in their composition when moving in sequential order from monosomes (F1) to heavy polysomes (F5; Figure 1–figure supplement 2B). Overall, these comparisons indicated that the experimental method was reproducible.

In unstressed conditions, 463 proteins were detected in all of F1-F5, and 516 in all of F1-F4 (Figure 1E-F). Fewer proteins were found in heavy polysomes during stress – 353 proteins were shared across F1-F4 in all three conditions, but only 141 of these were present in F5 as well (Figure 1E-F). The proteins found across F1-F4 included 70 ribosomal proteins (RPs), 25 translation factors and regulatory proteins (TFs), 240 other known RNA binding proteins (RBPs), as recently defined (Hentze et al. 2018), as well as 18 proteins that were not previously designated as RNA- or ribosome-binding (Figure 2A, Supplementary file 1–sheet 2).

A comparison of protein abundance in cytoplasmic extracts showed minimal change in label-free quantification (LFQ) intensity (Tyanova et al. 2016) between stressed and control samples, indicating that the dramatic ribosome run-off within 15 min following stress did not have sufficient time to impact the total cellular protein content and that our method sampled cells during their adaptive phase (Figure 1–figure supplement 2C). We also saw no evidence that either nascent protein chains or co-translational complex formation (Shiber et al. 2018) contributed significantly to the signal for our polysome-associated proteins. Cumulative amino- to carboxy-terminal peptide intensity profiles for individual proteins in total and polysome associated fractions showed no N-terminal bias in F1-F5 compared with T samples, except for rare examples (Figure 1–figure supplement 3, see Methods and figure legend for details).

For each protein, we estimated its percentage ribosome association by comparing abundance in the totals and the sum of the polysome fractions (see Methods; Figure 2A, Supplementary file 1–sheet 3). As expected, RPs and ribosome-associated chaperones (e.g.

Ssz1) were highly associated with ribosomes. In contrast, other proteins showed broad variations in ribosome association, from <2.5% to 100%. For abundant and transiently associating translation elongation factors, we estimate less than 20% of each protein was present in F1-F5, while all initiation factors except for the highly abundant eIF4A were over 30% ribosome-associated in unstressed cells. Known RBPs (yellow) and proteins not assigned to any other class (grey) showed highly varied ribosome association (Figure 2A), reflecting the large functional diversity within these categories. In response to both stresses, most TFs and related factors either reduced or maintained their overall ribosome association (Figure 2B). As there is a rapid attenuation in global translation initiation rates, as evidenced by polysome run off, reduced engagement of initiation factors is expected. Under conditions of glucose starvation or heat shock the RNA helicase eIF4A is rapidly dissociated from polysomes (Castelli et al. 2011; Bresson et al. 2020). In contrast, we observed no significant change in eIF4A or Ded1 association, indicating that loss of eIF4A is not a universal response to stress. In addition, a reduction of elongation rates accompanies oxidative stress (Shenton et al. 2006), with enhanced eEF2 phosphorylation (Wu et al. 2020). Here we find enhanced association of both eEF2 and eIF5A with ribosomes during both oxidative stress and amino acid starvation (Figure 2B). These findings are consistent with slowed translocation and enhanced ribosome pausing during stress. In summary, these stress-induced changes in the ribosome association of TFs are consistent with current ideas about how stress impacts the core translation machinery.

Ribosomal proteins typically respond uniformly to stress.

We were able to quantify 55 RPs across F1-F5 in stressed and unstressed cells (Supplementary file 1–sheet 2). In unstressed cells, ribosomal proteins were typically distributed evenly across the monosomal and polysomal fractions (F1-F5), but greater variation was observed during stress, especially in the fractions representing denser polysomes (Figure 3A). For example, Rpl38/eL38 was among the most polysome-enriched RPs during stress, with relatively high levels in F5, while under the same conditions Asc1/RACK1 stayed relatively evenly engaged and Rps2/uS5 was significantly depleted from F4-F5 relative to other RPs (Figure 3b).

We used unbiased hierarchical clustering of normalised LFQ intensities (‘polysome enrichment profiles’) to identify patterns among the 353 protein groups observed in F1-F4 in all conditions. This separated proteins into 14 clusters with variable F1-F4 and/or T enrichments in the presence and absence of stress (Figure 3c, Supplementary file 1–sheet 3). Proteins in clusters 1-3 exhibited low abundance in polysomes relative to totals, but maintained PE during both stresses. In contrast, those in clusters 11-14 were typically highly associated with ribosomes and enriched in heavier polysome fractions in unstressed

conditions, but shifted into monosome fractions following stress, in line with the global polysome profile (Figure 3c).

Almost all the RPs were found in clusters 11-12 and generally behaved similarly to Rps3/uS3, for example Asc1/RACK1 and Rpl38/eL38 (both cluster 12; Figure 3b), consistent with the idea that the RPs are responding in a concerted manner. Within these two clusters, there was some variation in the degree to which the different RPs shifted into monosomes during stress, for example Rps2/uS5 was relatively more depleted from heavy polysomes compared with Rps3/uS3 (Figure 3b). Only three RPs separated into other clusters. Rpl8b/uL8 and Rps10/eS10 (cluster 13) appear to be more depleted from heavy polysomes during stress, suggesting that they might be selectively lost from the mRNA-engaged pool of ribosomes during stress (Figure 3c). Conversely, Rpl7b/uL30 (cluster 6) retained PE during both stresses in a similar manner to mRNA-binding factors such as Pab1 (Figure 3c). Although a growing body of evidence suggests that variations in the association of specific RPs and paralogs with ribosomes contributes to mRNA-specific translation e.g. (Slavov et al. 2015; Ferretti et al. 2017; Gerst 2018; Cheng et al. 2019), our data did not provide strong evidence that variations in RP abundance were critical for these stress responses, so we did not explore the variation we observed among the RPs further. Instead we focused on accessory ribosome-associated proteins.

RBPs exhibit varied polysome association in response to stress.

Several recent genome-wide studies have defined yeast RBPs by cross-linking proteins to RNA and then identifying them by a MS approach or by an *in vitro* protein array (Mitchell et al. 2013; Beckmann et al. 2015; Matia-Gonzalez et al. 2015). Such studies have found proteins with typical RNA-binding domains (e.g. RRM, KH, PUF) as well as a range of proteins lacking classical domains, including numerous metabolic enzymes. A recent review concluded over 1200 yeast proteins had been identified as RBPs in high-throughput studies, with many found by multiple independent methods (Hentze et al. 2018). Here we identified over 240 polysome-associated RBPs in addition to the core RPs and TFs (Supplementary file 1–sheets 2 and 3). In contrast to the RPs, which form a relatively tight co-regulated group, RBPs are distributed across all 14 clusters, indicating they differ widely both in their percentage ribosome association (low in clusters 1-3, medium in 8-10 and high in the other clusters) and in how their PE changes in response to stress (Figure 3c). In contrast to the RPs, which generally became less abundant in heavier fractions during stress, proteins in clusters 1-3 and 8-9 were evenly spread across the fractions in both unstressed and stressed cells, while factors in clusters 4-6 and 10 became more enriched in the heavier polysome fractions during both stresses (Figure 3c, Supplementary file 1–sheet 3).

We reasoned that the factors remaining associated with polysomes during stress would likely include those acting to resolve the impact of stress at the translational level. For example, the multi-KH domain-containing protein Scp160 (cluster 4) is known to interact with polysomal mRNAs during both optimal growth conditions and during glucose starvation (Arribere et al. 2011). Scp160 behaved equivalently here following both 3-AT and H_2O_2 treatment (Figure 3c). A recent study proposed that Scp160 enhances the polysome association of codon-optimized transcripts by channelling or recycling tRNAs at ribosomes using successive synonymous codons (Hirschmann et al. 2014). Interestingly, aminoacyl tRNA synthetases (aaRSs) were enriched in clusters 2 and 3, which maintain PE during stress (Figure 3c).

Several RQC factors were identified in our dataset. For example, Mbf1 (cluster 3) is recruited to stalled disomes where it can prevent frameshifting of collided ribosomes (Wang et al. 2018). Similarly, Cdc48 (also cluster 3) is recruited to ribosomes to promote ubiquitination of stalled proteins (Defenouillere et al. 2013). In contrast Gcn1, which was recently shown to bind across both stalled and collided ribosome disome partners (Pochopien et al. 2021) and is necessary for activation of Gcn2 for eIF2 phosphorylation (Marton et al. 1997), is placed in cluster 9, which is evenly associated across polysome fractions under all conditions sampled (Figure 3c). In contrast, the ribosome-associated chaperone (RAC) complex members Zuo1 and Ssz1, follow the RP pattern in cluster 12. Thus various proteins associated with resolving stalled/collided ribosomes have distinct patterns of PE following these stresses, likely reflecting their individual roles in RQC.

Cytosolic aspartate aminotransferase moderates the ISR

Gene ontology analysis revealed that many of the most highly polysome-enriched proteins were metabolic enzymes, including glycolytic enzymes (e.g. Pgk1, Fba1, Eno1) and amino acid biosynthetic enzymes (e.g. Met6, His4, Trp5) (Figure 3c, Figure 3–figure supplement 1, Supplementary file 1–sheet 4). While their association with mRNA is known (Supplementary file 1–sheet 3), their additional roles (if any) remain unclear. To investigate whether any of these RBPs, which retain or increase their ribosome association and PE during stress (clusters 1-6 and 8-10), function in the stress response, we screened a selection of single gene deletion strains for growth phenotypes in the presence of H_2O_2. We found that deletion of *AAT2*, the cytosolic aspartate amino transferase, conferred an H_2O_2-hypersensitive growth phenotype (Figure 4A, Figure 4–figure supplement 1A). Polysome profile analysis revealed that translation was similar in untreated *aat2*Δ and wild-type (parent) cells, but ribosome run-off caused by addition of H_2O_2 was more acute in *aat2*Δ at lower concentrations of peroxide (Figure 4b, Figure 4–figure supplement 1B). This is consistent with reduced translation initiation in *aat2*Δ contributing to hydrogen peroxide growth sensitivity, suggesting that Aat2

has a role in translational regulation in response to stress. As phosphorylation of eIF2α by Gcn2 is responsible for ribosome run-off following oxidative stress (Shenton et al. 2006), we used phospho-specific antibodies to assess the state of eIF2α in whole cell extracts, which showed heightened phosphorylation in response to lower concentrations of H_2O_2 in *aat2*Δ cells (Figure 5A). The ISR in yeast is mediated via translational control of the transcription factor *GCN4*. The four upstream open reading frames (uORFs) in the long *GCN4* 5' leader limit translation of the main ORF, except where elevated eIF2α phosphorylation inhibits its nucleotide exchange factor eIF2B, enabling uORF skipping and higher Gcn4 expression. We used the well-established *LacZ* reporter plasmid (p180) to indirectly monitor Gcn4 levels in these cells (Hinnebusch 2005), which confirmed that *aat2*Δ cells had higher LacZ levels following 2 hours of peroxide stress (Figure 5b). Control reporter plasmids bearing single or no uORFs were not changed from the parent strain (Figure 5b), suggesting there is no defect in mRNA levels, scanning or re-initiation proficiency on the *GCN4* leader. The data indicate that the yeast ISR is aberrantly activated by H_2O_2 when Aat2 is deleted.

Aat2 binds 60S ribosomes

Our polysomal proteomics estimated that 8-10% of Aat2 was ribosome-associated (Figure 2A, Supplementary file 1–sheet 3). A strain bearing a C-terminal TAP tag behaved similarly, with the majority of the tagged protein retained at the top of a sucrose gradient and only 10% present in fractions 5-9 (which correspond to the fractions analysed by MS; Figure 6A). Comparable PE was observed with both western blotting with Aat2-TAP and MS with the untagged protein for H_2O_2-treated samples (13% and 9%, respectively; Figure 6a, Supplementary file 1–sheet 3).

To investigate whether polysome-associated Aat2 was primarily ribosome- or mRNA-bound or part of another high-molecular weight complex, we separated ribosome-bound proteins from free proteins on sucrose cushion gradients and analysed the pellet fraction on new polysome gradients with or without treatment with RNase I. In the absence of RNase I, Aat2 and control mRNA-binding proteins Pab1 and Scp160 were all polysome-associated (Figure 6b). Following RNase I treatment, the mRNA-binding factors migrated at the top of the gradient, while Aat2 was predominantly 80S-associated, indicating it is principally a ribosome-associated factor rather than an mRNA-binding protein (Figure 6b, lanes 5-6). This also ruled out the possibility that Aat2 was present in polysome fractions through an association with another large cytoplasmic complex. EDTA treatment to separate the ribosomal subunits further indicated that Aat2 predominantly binds to 60S (large) ribosomal subunits (Figure 6c, lanes 8-10).

RE and stress sensitivity are independent of Aat2 aspartate aminotransferase function. Aat2 is a cytosolic aspartate aminotransferase enzyme that catalyses the reversible transamination reaction: *2-oxoglutarate* + *L-aspartate* ↔ *L-glutamate* + *oxaloacetate*. By interconverting *L*-aspartate and oxaloacetate, the enzyme links amino acid and carbohydrate metabolism (Figure 7–figure supplement 1A). Aat2 has a paralog, Aat1, which performs the same reactions within mitochondria, although the cytosolic form is the major contributor of total aspartate aminotransferase activity (Blank et al. 2005). When grown on minimal medium, the *aat2*Δ mutant is an aspartic acid auxotroph, but when amino acids are supplied, as here in our experiments, cells grow well as Aat2 enzymatic function is not required (Figure 7–figure supplement 1B). To determine if the polysome-associated role of Aat2 in the stress response can be separated from its role in metabolism, we used the crystal structure of the Aat2 homodimer (PDB 1YAA (Jeffery et al. 1998)) and its homology to other aspartate aminotransferases (Winefield et al. 1995) to identify active site residues K255 and R387, which engage the cofactor pyridoxal-5'-phosphate and the active site competitive inhibitor maleate, respectively (Figure 7A). We used a CRISPR/Cas9-mediated approach to introduce glutamic acid charge reversal mutations individually at these two positions in *AAT2-TAP* cells, and created a control containing four silent mutations in the guide RNA binding sequence (SM). Importantly, both K255E and R387E mutations conferred aspartic acid auxotrophy (Figure 7–figure supplement 1B), despite being expressed well (Figure 7–figure supplement 1C), and retained ribosome binding activity (Figure 7b), showing that they compromise aspartate aminotransferase enzyme function, but not expression or ribosome-binding activity. All three versions of Aat2-TAP maintained the same polysome responses to oxidative stress (Figure 7C), unlike *aat2*Δ cells which had enhanced H_2O_2 sensitivity (Figure 4C) and the Aat2 mutant proteins all migrate into polysomes in both stressed and unstressed cells (Figure 7D). Taken together, these observations indicate that the ribosome/polysome-binding and aspartate aminotransferase enzyme functions of Aat2 are separable activities and that Aat2 can modulate the yeast ISR.

Discussion

Polysome proteomics

Our polysomal proteomics approach (Figure 1) captures many aspects of translation and its regulation by stress, including the behaviour of ribosomal proteins, initiation factors, elongation factors and RNA-binding proteins (Figures 2 and 3). Our unbiased clustering reveals that proteins displaying common changes in polysome association profiles across unstressed and stressed conditions share common functions in translational control. These shared regulatory responses likely result from the reductions in growth rates and global translation initiation and elongation activity that occur (Figure 1). As expected, when global translation initiation was reduced, initiation factors reduced in relative polysome association during stress. This applied to almost all, with the exception of the RNA helicases Ded1, eIF4A and its associated eIF4B, and the 60S joining factor eIF5B (Figure 2). The RNA helicases associated with polysomes equally in unstressed and stressed cells. This is perhaps surprising, because eIF4A, eIF4B and Ded1 were found to be rapidly lost from polysomes following both glucose starvation and heat shock (Castelli et al. 2011; Bresson et al. 2020). Perhaps importantly, neither glucose withdrawal for 10-15 min nor the immediate response to heat shock requires eIF2α phosphorylation (Ashe et al. 2000; Grousl et al. 2009; Castelli et al. 2011). eIF4A has at least two separate roles in yeast translation: first, it contributes to the recruitment of the 43S pre-initiation complex (PIC) to the 5' end of capped mRNAs, and second it helps to unwind mRNA secondary structures during scanning towards the AUG start codon (Yourik et al. 2017; Merrick and Pavitt 2018). Here, the mRNA cap-binding factor eIF4E and its partner eIF4G were the most ribosome-depleted initiation factors during stress (Figure 2), while their global RNA-binding was found to be unchanged following glucose starvation or heat stress (Bresson et al. 2020). It was also noted previously that protein-protein interactions among these 5' cap-associated factors were not altered by stress, but that interactions with specific mRNAs were changed when these were quantified by a RNA-immunoprecipitation and RNA-sequencing approach (Costello et al. 2017). Together these data are consistent with models where hydrogen peroxide and amino acid starvation act at early time points via enhanced eIF2α phosphorylation to reduce 43S PIC-mRNA association, while heat shock and glucose starvation instead retain these 43S PIC-mRNA interactions, but act to impede the subsequent scanning step via selective loss of RNA helicases.

In addition to impacting translation initiation, both stresses we investigated impair translation elongation (Shenton et al. 2006; Harding et al. 2019; Wu et al. 2020). Stalled/collided ribosomes are proposed to activate Gcn2 (Pochopien et al. 2021), so this logically precedes the rapid attenuation of initiation. Slower migration of ribosomes increases ribosome density (Yu et al. 2015). We observed increased interactions of both eEF2 (*EFT2*)

and eIF5A (*HYP2*) with ribosomes during stress (Figure 2). eEF2 (cluster 2) promotes ribosomal translocation and its PE was maintained under all conditions (Figure 3). Enhanced eEF2 phosphorylation during oxidative stress (Wu et al. 2020) may reduce its activity and lead to the higher ribosome interaction we observe. In contrast, eIF5A (cluster 11, Figure 3) binds to the ribosomal exit site to promote peptide bond formation on stalled or paused 80S ribosomes, and has recently been observed in Gcn1-bound disome structures (Schuller et al. 2017; Pochopien et al. 2021). Thus the increased association of eIF5A with ribosomes makes mechanistic sense in the context of stress-induced ribosome pauses.

The ribosomal proteins generally behaved coherently in their polysome association in our data, becoming highly enriched in the monosomal fraction (F1) during both oxidative stress and histidine starvation, consistent with most ribosomes remaining intact (Figure 3). However, differences in the degree to which some RPs became monosome-enriched during stress were observed. Rpl8b/uL8 and Rps10/eS10 (cluster 13, Figure 3) were both more depleted from the heavy polysome fractions (F4-F5) during stress than the other RPs, suggesting that they might be selectively depleted from the mRNA-engaged pool of ribosomes under these conditions. Rpl8 has been implicated in contributing to 60S biogenesis: the absence of Rpl8 causes the depletion of several large subunit RPs and ribosome assembly factors from pre-ribosomes, including Rpl28/uL15 (cluster 12) (Jakovljevic et al. 2012). Rps10 is located within the mRNA entry channel and contacts mRNA during translation. It is commonly mutated in Diamond-Blackfan Anemia, an inherited bone marrow failure syndrome (Doherty et al. 2010). A recent study showed that the ribosome assembly factor Ltv1 promotes the incorporation of Rps10, Rps3 and Asc1 into the 40S head and that *ltv1*Δ cells have growth defects, including enhanced sensitivity to oxidative stress (Collins et al. 2018). The mammalian ortholog of Rps10 is a target for ZNF598 (the homolog of Hel2) ubiquitination (Garzia et al. 2017). Yeast Rps10 can also be ubiquitinated (Swaney et al. 2013), so partial ubiquitination of Rps10 might explain its reduced detection by MS in heavy polysomes. The four other members of cluster 13 (Dbp2, Nmd3, Arb1, Arx1) are involved in ribosome biogenesis, nonsense-mediated decay (NMD) or RQC (Woolford and Baserga 2013), consistent with their strong depletion from heavy polysomes in both unstressed and stressed conditions.

Uniquely among RPs, Rpl7b/uL30 was placed in cluster 6 along with mRNA-binding factors such as Pab1, which remained polysome-enriched during both stresses. Isoform-specific roles have been investigated for this paralog pair, with potential differential impacts on Ty element transposition described (Palumbo et al. 2017). In our MS data the signal for Rpl7a (thought to be the major isoform) differed from that for Rpl7b, peaking in F5 in unstressed cells and F2 (disome/trisomes) during both stresses (Supplementary file 1–sheet 2). Further dedicated studies will be needed to determine whether these RPs have specific roles in stress responses.

Aat2 alters the sensitivity of the ISR to oxidative stress

Here we identified Aat2 as a ribosome binding factor modulating the oxidative stress sensitivity of yeast cells. Loss of Aat2 enhances both stress sensitivity and the activation of the eIF2 kinase Gcn2 (Figures 4 and 5). In yeast, Gcn2 is the sole eIF2 kinase activating the ISR (Hinnebusch 2005; Pavitt 2018). Previously it was found that mutations in ribosomal proteins or associated factors can modulate Gcn2 activation. For example, deletion of *RPS10A* or *RPS10B* (both encoding eS10) limits the activation of Gcn2 kinase in replete conditions and following amino acid starvation (Lee et al. 2015), thus slowing activation of the ISR. Rps10 was found to contact Gcn1 in yeast two-hybrid experiments, suggesting that the RP can modify the sensitivity of Gcn1, a factor which is necessary for Gcn2 activation (Lee et al. 2015). In contrast, loss of the RQC factor Hel2 promotes or enhances eIF2α phosphorylation both in unstressed cells and in response to the alkylating agent MMS (Yan and Zaher 2021). Hel2 is an E3 ligase that ubiquitinates Rps20/uS10 and Rps3/uS3 (both cluster 12) in response to ribosome stalling to initiate RQC (Matsuo et al. 2017). Since RQC is inhibited in the absence of Hel2 and the Gcn2 activator Gcn1 binds to stalled/collided disomes, these findings suggested a model whereby Hel2 helps to resolve moderate stalls, and that Gcn2 activation ensues when Hel2 is unable to act or is overwhelmed during stress (Yan and Zaher 2021). We observed heightened eIF2α phosphorylation at low H_2O_2 levels after only 15 minutes of treatment in *aat2*Δ cells (Figure 4), which resembles these recent *hel2*Δ observations under similar stress conditions. Aat2 (Figure 6) and Gcn2 (Ramirez et al. 1991; Inglis et al. 2019) both bind to 60S ribosomal subunits, suggesting a potential model where Aat2 binding to polysomal 60S subunits can antagonise Gcn2 activation. At present we cannot say how direct the role of Aat2 is, only that it appears upstream of Gcn2. Aat2 functions in amino acid metabolism as one of two enzymes that interconvert aspartate and glutamate, so we performed our studies under conditions where amino acid supply is in excess and its aspartate aminotransferase function is not essential. Two mutants that target key residues for catalytic function remain able to bind translating ribosomes and do not show the translational control phenotype of *aat2*Δ (Figure 7). These results imply that the translational control role of Aat2 is independent of its aspartate aminotransferase function.

Enzymes with secondary roles have been termed 'moonlighting enzymes' (Castello et al. 2015) and those that bind RNA have been proposed to act as a post-transcriptional network linking metabolism to gene regulation (Hentze and Preiss 2010). The best-studied example of an RNA-binding metabolic enzyme is IRP1. In the presence of iron, IRP1 functions independently of RNA as the enzyme aconitase, while in the absence of iron it instead binds to specific target mRNAs via stem loop structures known as iron response elements, thus

493 regulating their stability or translation. Other examples from glycolysis and other metabolic
494 pathways have been reviewed elsewhere (Hentze and Preiss 2010). However, as far as we
495 are aware, Aat2 is the first example of a metabolic enzyme that binds to ribosomes and
496 modulates the integrated stress response.

Methods

Key resources table

Reagent type (species) or resource	Designation	Source or reference	Identifiers	Additional information
antibody	IRDye 800CW Goat anti-Rabbit IgG (H + L)	LI-COR Biosciences	Cat. no.: 926-32211	Used at 1/10,000 dilution
antibody	IRDye 680RD Goat anti-Mouse IgG (H + L)	LI-COR Biosciences	Cat. no.: 926-68070	Used at 1/10,000 dilution
antibody	IRDye 680RD Donkey anti-Chicken IgG (H + L)	LI-COR Biosciences	Cat. no.: 926-68075	Used at 1/10,000 dilution
chemical compound, drug	Hydrogen peroxide solution	Sigma	Cat. no.: 95321	Made 1/100 dilution in water before adding to cultures/media
chemical compound, drug	3-amino-1,2,4-triazole	Sigma	Cat. no.: A8056	
peptide, recombinant protein	Ambion RNase I	Thermo Fisher	Cat. no.: AM2294	
peptide, recombinant protein	Sequencing Grade Modified Trypsin	Promega	Cat. no.: V5111	
commercial assay or kit	NuPAGE 4 to 12%, Bis-Tris, 1.0 mm, Mini Protein Gel, 12-well	Life Technologies	Cat. no.: NP0322	
strain, strain background (*E. coli*)	XL10-Gold Ultracompetent Cells	Agilent	Cat. no.: 200314	
software, algorithm	LI-COR Image Studio and LI-COR Image Studio Lite	LI-COR Biosciences	https://www.licor.com/bio/software	Version 5.2. LI-COR Image Studio Lite has since been discontinued.
software, algorithm	R	R Core Team, 2019	https://www.r-project.org/	Version 3.6.2
software, algorithm	MaxQuant	Tyanova et al, 2016	https://www.maxquant.org/	Version 1.5.7.4
software, algorithm	GNU Image Manipulation Program	GIMP	https://www.gimp.org/	Version 2.8.10

499

500 **Yeast strains**

501 Yeast strains used in this study are described in Supplementary file 1–sheet 5. Plasmids are
502 described in Supplementary file 1–sheet 6. All strains used were from the BY4741
503 background. Strains made in this study were constructed using standard yeast transformation
504 and site-directed mutagenesis using the CRISPR/Cas9 system (Anand et al. 2017).
505 Oligonucleotides used to make mutations or confirm gene deletions or mutations are listed in
506 Supplementary file 1–sheet 7.

507 **Cell growth conditions**

508 *S. cerevisiae* colonies were inoculated into 5 mL synthetic complete medium containing
509 dextrose (2%) lacking histidine (SC –His) and grown overnight at 30°C with rotation at 180
510 rpm. The next day, 200 mL cultures were started at an OD_{600} of 0.1. For oxidative stress
511 experiments, hydrogen peroxide (H_2O_2) was added during exponential growth (OD_{600} 0.6-1.0)
512 at a final concentration of 0.2-0.8 mM. For histidine starvation, 3-amino-1,2,4-triazole (3-AT)
513 was added during exponential phase at a final concentration of 10 mM.

514 **Site-directed mutagenesis**

515 Two point mutations were separately introduced into AAT2-TAP using the CRISPR/Cas9
516 system. A guide RNA targeting the *AAT2* coding sequence was designed using the ATUM
517 web tool (https://www.atum.bio/eCommerce/cas9/input) and cloned into plasmid pAV2676,
518 containing the *Cas9* gene under the control of the *PGK1* promoter (Supplementary file 1–
519 sheet 6). Three repair oligonucleotides were designed to target repair to the *AAT2* locus and
520 generate point mutants: control, K255E and R387E (Supplementary file 1–sheet 7). Each
521 contained four silent mutations within the guide RNA target sequence to ensure the locus was
522 not re-cut following repair, without changing the amino acid sequence. The *Cas9*/guide RNA
523 plasmid and repair construct oligonucleotide were simultaneously transformed into the *AAT2-*
524 *TAP* strain (GP7542) and transformants selected by plating on SC –Leu. Transformants were
525 screened by sequencing (Eurofins Genomics) to confirm the presence of the correct mutations
526 and the *Cas9*/guide RNA plasmid was removed by growth on SC medium.

527 **Serial dilution growth spotting assays**

528 *S. cerevisiae* cultures were grown to exponential phase then diluted to OD_{600} 0.1 in sterile
529 water in a 96-well plate. A dilution series was made for each strain in sterile water to give
530 cultures at OD_{600} 0.1, 0.01, 0.001 and 0.0001. Two microliters of each culture were plated on
531 to SC and SC +H_2O_2 (final H_2O_2 concentrations 0.4-2.0 mM) agar plates. Plates were
532 incubated at 30°C or 37°C and imaged after 48 hours.

533 **Polysome profiling**

534 Cultures were grown at 30°C to an OD_{600} of 0.6-1.0. Formaldehyde crosslinking was used to
535 fix translating ribosomes and their associated factors on mRNA. Cultures were transferred into

pre-chilled Falcon tubes containing formaldehyde (at a final concentration of 0.8% (v/v)) and a quarter volume of frozen media pellets. Samples were incubated on ice for 1 h then excess formaldehyde was quenched by the addition of 2 M glycine (final concentration 80 mM). Cells were harvested by centrifugation, washed and lysed with acid-washed glass beads in 200 µL polysome lysis buffer (20 mM HEPES pH 7.4, 2 mM magnesium acetate, 100 mM potassium acetate, 0.5 mM DTT, 0.1% DEPC) for 20 s, 7 times.

Two OD units of lysate were layered on to 15-50% sucrose gradients prepared in 12 mL thin-walled open polyallomer tubes (Seton Scientific) and separated by ultracentrifugation in an SW41 Ti rotor (2.5 h at 278,000 x *g*, 4°C). Profiles were generated by continuous A_{254} recording using a UA-6 UV/Vis detector and chart recorder (Teledyne ISCO). Profile images were analysed using GNU Image Manipulation Program (version 2.8.10). Monosomal and polysomal fractions were collected manually at pre-determined intervals. For limited RNase digestion, 1 U/µL RNase I (Ambion) was added to lysates prior to polysome profiling and incubated for 30 min at room temperature. For EDTA treatment, 50 mM EDTA was added to lysates and incubated for 30 min on ice.

Sucrose cushions

Lysates were prepared as for polysome profiling. 16 OD units of lysate (normalised to 500 µL volume) were layered without mixing on top of 400 µL of 36% sucrose in polysome lysis buffer, in thick-walled open polycarbonate tubes (Beckman Coulter) and separated by ultracentrifugation in a TLA120.2 rotor (Beckman Coulter; 1.5 h at 278,000 x *g*, 4°C).

For polysome profiling, supernatants were concentrated in Amicon Ultra 3 kDa MW cut-off centrifugal concentrators (Millipore) and ribosome pellets were resuspended in polysome lysis buffer. For western blotting, protein was extracted from supernatants and pellets were resuspended directly in protein loading buffer (2x NuPAGE LDS sample buffer (Invitrogen), 715 mM 2-mercaptoethanol). Samples were incubated for 5 min at 95°C.

Protein extraction

Protein was extracted from sucrose gradient fractions for analysis by western blotting and MS. A half volume of ice-cold 40% TCA was added to each fraction, mixed by inversion and incubated overnight at -20°C. Precipitated protein was pelleted by centrifugation (15 min at 20,000 x *g*, 4°C) and washed twice with ice-cold acetone. Pellets were dried for 20 min at room temperature then resuspended in 5 µL of 1 M Tris and 10 µL of protein loading buffer (2x NuPAGE LDS sample buffer (Invitrogen), 715 mM 2-mercaptoethanol). Samples were incubated for 5 min at 95°C.

SDS-PAGE & western blotting

Protein samples were resolved on NuPAGE 4-12% Bis-Tris gels (Invitrogen) and transferred to nitrocellulose membranes. Membranes were probed with monoclonal and polyclonal

antibodies listed in Supplementary file 1–sheet 8 and visualised using LI-COR fluorescent secondary antibodies. Bands were quantified using LI-COR Image Studio (version 5.2).

Label-free MS

Protein samples from sucrose gradient fractions and cytoplasmic extracts ('totals') were dehydrated using acetonitrile and centrifuged under vacuum. Dried gel pieces were reduced with 10 mM DTT and alkylated with 55 mM iodoacetamide, then twice washed alternately with 25 mM ammonium bicarbonate and acetonitrile. Gel pieces were dried by vacuum centrifugation and samples digested using trypsin overnight at 37°C.

Liquid chromatography (LC) was carried out using an UltiMate 3000 Rapid Separation Binary System (Thermo Fisher Scientific). Peptides were concentrated using an ACQUITY UPLC M-Class Symmetry C18 Trap Column (180 µm inner diameter, 20 mm length (Waters)) and then separated using an ACQUITY UPLC M-Class Peptide BEH C18 Column (75 µm inner diameter, 250 mm length, 1.7 µm particle size (Waters)). A gradient starting with 99% Buffer A (0.1% formic acid in water) and 1% Buffer B (0.1% formic acid in acetonitrile) and increasing to 75% Buffer A and 25% Buffer B was used to separate the peptides over 45 min at a flow rate of 200 nL/min. Label-free tandem MS was performed using an Orbitrap Elite Hybrid Ion Trap-Orbitrap Mass Spectrometer (Thermo Fisher Scientific). Peptides were selected for fragmentation and MS2 analysis automatically by data-dependent analysis.

MS data processing

Raw MS data were processed using MaxQuant version 1.5.7.4 (Tyanova et al. 2016). A peptide mass tolerance of 20 ppm was used for the first search, 4.5 ppm for the main search, and 0.5 Da for the MS/MS fragment ions. The peak list was searched against the Uniprot *Saccharomyces cerevisiae* database (accessed 10th February 2017) using the built-in Andromeda search engine (Cox et al. 2011). 901 protein groups were identified in two or more replicates for at least one sample (F1-F5 or T, Supplementary file 1–sheet 1). Of these, 840 were uniquely identified proteins encoded by single genes, while 61 are 'grouped' proteins that are not distinguishable by MS (most of which are RP paralog pairs). Throughout the text 'protein' is used to refer to both grouped and uniquely identified proteins.

Processed label-free data were analysed and presented using R (version 3.6.2) (R Core Team 2019) and additional packages therein. LFQ intensity values from MaxQuant were used as the primary quantitative signal. To generate 'polysome enrichment profiles', LFQ intensities were $\log_2$-transformed and normalised for each protein to its mean across the unstressed gradient fractions (F1-F5).

The overall ribosomal engagement of each protein was estimated by summing the raw LFQ intensities in the gradient fractions (fraction sum, FS) then calculating the $\log_2$-transformed FS/T ratio for each condition. This was then used to estimate the percentage ribosome association of each protein by comparing the FS/T ratio to that which would be

609 expected if all of the protein was present in F1-F5, based on the relative loading amounts: for
610 a protein which was entirely located in F1-F5 during sucrose gradient fractionation, the
611 expected raw LFQ intensity was 30 times higher for the fraction sum than the total (equivalent
612 to $\log_2$-transformed FS/T = 4.91). Therefore, %P = (FS/T) / 30 * 100 (where FS/T has been
613 inverse $\log_2$-transformed first).
614 Hierarchical clustering was used to identify sets of proteins with similar 'polysome
615 association profiles' using the R functions *dist* (method: 'euclidean') and *hclust* (method:
616 'complete').
617 To assess the contribution of nascent peptides to MS signal, cumulative peptide
618 intensity from N- to C-terminus was calculated for proteins with a greater than median number
619 of peptides and sequence coverage. Cumulative peptide intensity distributions from sucrose
620 gradient fractions were compared with those from totals using the Kolmogorov-Smirnov test
621 (with Bonferroni correction).
622 **β-galactosidase assays**
623 β-galactosidase activity was measured in strains transformed with *GCN4-lacZ* plasmids to
624 assay the translational induction of *GCN4* during oxidative stress as described (Dever 1997).
625 Strains were grown to exponential phase in 50 mL SC –uracil. Cells were harvested by
626 centrifugation, washed and lysed with acid-washed glass beads in 200 µL of breaking buffer
627 (0.1 M Tris pH 8, 20% glycerol, 1 mM 2-mercaptoethanol) for 20 s, 5 times. Another 200 µL of
628 breaking buffer was added and mixed by vortexing. Samples were cleared by centrifugation
629 to remove cell debris (10 min at 7000 x *g*, 4°C). β-galactosidase activity was measured for
630 100 µL lysate mixed with 900 µL of Z-buffer (60 mM sodium phosphate dibasic heptahydrate,
631 45 mM sodium phosphate monobasic, 10 mM potassium chloride, 2 mM magnesium sulphate,
632 40 mM 2-mercaptoethanol). Samples were incubated for 10 min at 28°C and reactions started
633 by adding 200 µL ONPG (4 mg/mL in Z-buffer). Reactions were stopped by the addition of
634 500 µL 1 M sodium carbonate and A_{405} was measured.
635 **Data availability**
636 The mass spectrometry proteomics data have been deposited to the ProteomeXchange
637 Consortium via the PRIDE (Perez-Riverol et al. 2019) partner repository with the dataset
638 identifier PXD027903.
639 Reviewer account details to access data:
640 Website: http://www.ebi.ac.uk/pride
641 Username: reviewer_pxd027903@ebi.ac.uk
642 Password: 5stHjG9Y
643 **Funding**

644 RAC was supported by a BBSRC doctoral training partnership grant awarded to the University
645 of Manchester (BB/M011208/1). Additional funding support was provided from the Weizmann-
646 UK Joint Research Program to GDP (2020/129488).
647

648 **Acknowledgements**
649 We thank David Knight and colleagues at the University of Manchester BioMS Core Facility
650 (RRID:SCR_020987) for processing mass spectrometry samples and their helpful advice, and
651 Martin Jennings and Chris Kershaw for helpful advice and feedback throughout the study.
652

653 **Author contributions**
654 RAC: Conceptualization, Investigation, Data curation, Writing - original draft, Writing - review
655 and editing. No competing interests.
656 MPA: Conceptualization, Supervision, Writing - review and editing. No competing interests.
657 SJH: Conceptualization, Supervision, Writing - review and editing. No competing interests.
658 GDP: Conceptualization, Supervision, Funding acquisition, Project administration, Writing -
659 original draft, Writing - review and editing. No competing interests.
660

References

Adomavicius T, Guaita M, Zhou Y, Jennings MD, Latif Z, Roseman AM, Pavitt GD (2019) **The structural basis of translational control by eif2 phosphorylation** *Nat Commun* 10: 2136 https://doi.org/10.1038/s41467-019-10167-3

Aebersold R, Mann M (2016) **Mass-spectrometric exploration of proteome structure and function** *Nature* 537: 347-355 https://doi.org/10.1038/nature19949

Anand R, Beach A, Li K, Haber J (2017) **Rad51-mediated double-strand break repair and mismatch correction of divergent substrates** *Nature* 544: 377-380 https://doi.org/10.1038/nature22046

Arribere JA, Doudna JA, Gilbert WV (2011) **Reconsidering movement of eukaryotic mrnas between polysomes and p bodies** *Mol Cell* 44: 745-758 https://doi.org/10.1016/j.molcel.2011.09.019

Ashe MP, De Long SK, Sachs AB (2000) **Glucose depletion rapidly inhibits translation initiation in yeast** *Mol Biol Cell* 11: 833-848.

Beckmann BM, Horos R, Fischer B, Castello A, Eichelbaum K, Alleaume AM, Schwarzl T, Curk T, Foehr S, Huber W, Krijgsveld J, Hentze MW (2015) **The rna-binding proteomes from yeast to man harbour conserved enigmrbps** *Nat Commun* 6: 10127 https://doi.org/10.1038/ncomms10127

Blank LM, Lehmbeck F, Sauer U (2005) **Metabolic-flux and network analysis in fourteen hemiascomycetous yeasts** *FEMS Yeast Res* 5: 545-558 https://doi.org/10.1016/j.femsyr.2004.09.008

Bresson S, Shchepachev V, Spanos C, Turowski TW, Rappsilber J, Tollervey D (2020) **Stress-induced translation inhibition through rapid displacement of scanning initiation factors** *Mol Cell* 80: 470-484 e478 https://doi.org/10.1016/j.molcel.2020.09.021

Castelli LM, Lui J, Campbell SG, Rowe W, Zeef LA, Holmes LE, Hoyle NP, Bone J, Selley JN, Sims PF, Ashe MP (2011) **Glucose depletion inhibits translation initiation via eif4a loss and subsequent 48s preinitiation complex accumulation, while the pentose phosphate pathway is coordinately up-regulated** *Mol Biol Cell* 22: 3379-3393 https://doi.org/10.1091/mbc.E11-02-0153

Castello A, Hentze MW, Preiss T (2015) **Metabolic enzymes enjoying new partnerships as rna-binding proteins** *Trends Endocrinol Metab* 26: 746-757 https://doi.org/10.1016/j.tem.2015.09.012

Cheng Z, Mugler CF, Keskin A, Hodapp S, Chan LY, Weis K, Mertins P, Regev A, Jovanovic M, Brar GA (2019) **Small and large ribosomal subunit deficiencies lead to distinct gene expression signatures that reflect cellular growth rate** *Mol Cell* 73: 36-47 e10 https://doi.org/10.1016/j.molcel.2018.10.032

Collins JC, Ghalei H, Doherty JR, Huang H, Culver RN, Karbstein K (2018) **Ribosome biogenesis factor ltv1 chaperones the assembly of the small subunit head** *J Cell Biol* 217: 4141-4154 https://doi.org/10.1083/jcb.201804163

Costa-Mattioli M, Walter P (2020) **The integrated stress response: From mechanism to disease** *Science* 368 https://doi.org/10.1126/science.aat5314

Costello JL, Kershaw CJ, Castelli LM, Talavera D, Rowe W, Sims PFG, Ashe MP, Grant CM, Hubbard SJ, Pavitt GD (2017) **Dynamic changes in eif4f-mrna interactions revealed by global analyses of environmental stress responses** *Genome Biol* 18: 201 https://doi.org/10.1186/s13059-017-1338-4

Cox J, Neuhauser N, Michalski A, Scheltema RA, Olsen JV, Mann M (2011) **Andromeda: A peptide search engine integrated into the maxquant environment** *J Proteome Res* 10: 1794-1805 https://doi.org/10.1021/pr101065j

Crawford RA, Pavitt GD (2019) **Translational regulation in response to stress in saccharomyces cerevisiae** *Yeast* 36: 5-21 https://doi.org/10.1002/yea.3349

D'Orazio KN, Green R (2021) **Ribosome states signal rna quality control** *Mol Cell* 81: 1372-1383 https://doi.org/10.1016/j.molcel.2021.02.022

Defenouillere Q, Yao Y, Mouaikel J, Namane A, Galopier A, Decourty L, Doyen A, Malabat C, Saveanu C, Jacquier A, Fromont-Racine M (2013) **Cdc48-associated complex bound to 60s particles is required for the clearance of aberrant translation products** *Proc Natl Acad Sci U S A* 110: 5046-5051 https://doi.org/10.1073/pnas.1221724110

Dever TE (1997) **Using gcn4 as a reporter of eif2 alpha phosphorylation and translational regulation in yeast** *Methods* 11: 403-417 https://doi.org/10.1006/meth.1996.0437

Dever TE, Green R (2012) **The elongation, termination, and recycling phases of translation in eukaryotes** *Cold Spring Harb Perspect Biol* 4: a013706 https://doi.org/10.1101/cshperspect.a013706

Dever TE, Kinzy TG, Pavitt GD (2016) **Mechanism and regulation of protein synthesis in saccharomyces cerevisiae** *Genetics* 203: 65-107 https://doi.org/10.1534/genetics.115.186221

Doherty L, Sheen MR, Vlachos A, Choesmel V, O'Donohue MF, Clinton C, Schneider HE, Sieff CA, Newburger PE, Ball SE, Niewiadomska E, Matysiak M, Glader B, Arceci RJ, Farrar JE, Atsidaftos E, Lipton JM, Gleizes PE, Gazda HT (2010) **Ribosomal protein genes rps10 and rps26 are commonly mutated in diamond-blackfan anemia** *Am J Hum Genet* 86: 222-228 https://doi.org/10.1016/j.ajhg.2009.12.015

Ferretti MB, Ghalei H, Ward EA, Potts EL, Karbstein K (2017) **Rps26 directs mrna-specific translation by recognition of kozak sequence elements** *Nat Struct Mol Biol* 24: 700-707 https://doi.org/10.1038/nsmb.3442

Fleischer TC, Weaver CM, McAfee KJ, Jennings JL, Link AJ (2006) **Systematic identification and functional screens of uncharacterized proteins associated with eukaryotic ribosomal complexes** *Genes Dev* 20: 1294-1307 https://doi.org/10.1101/gad.1422006

Garzia A, Jafarnejad SM, Meyer C, Chapat C, Gogakos T, Morozov P, Amiri M, Shapiro M, Molina H, Tuschl T, Sonenberg N (2017) **The e3 ubiquitin ligase and rna-binding protein znf598 orchestrates ribosome quality control of premature polyadenylated mrnas** *Nat Commun* 8: 16056 https://doi.org/10.1038/ncomms16056

Gerst JE (2018) **Pimp my ribosome: Ribosomal protein paralogs specify translational control** *Trends Genet* 34: 832-845 https://doi.org/10.1016/j.tig.2018.08.004

Grousl T, Ivanov P, Frydlova I, Vasicova P, Janda F, Vojtova J, Malinska K, Malcova I, Novakova L, Janoskova D, Valasek L, Hasek J (2009) **Robust heat shock induces eif2alpha-phosphorylation-independent assembly of stress granules containing eif3 and 40s ribosomal subunits in budding yeast, saccharomyces cerevisiae** *J Cell Sci* 122: 2078-2088 https://doi.org/10.1242/jcs.045104

Harding HP, Ordonez A, Allen F, Parts L, Inglis AJ, Williams RL, Ron D (2019) **The ribosomal p-stalk couples amino acid starvation to gcn2 activation in mammalian cells** *Elife* 8 https://doi.org/10.7554/eLife.50149

Hentze MW, Castello A, Schwarzl T, Preiss T (2018) **A brave new world of rna-binding proteins** *Nat Rev Mol Cell Biol* 19: 327-341 https://doi.org/10.1038/nrm.2017.130

Hentze MW, Preiss T (2010) **The rem phase of gene regulation** *Trends Biochem Sci* 35: 423-426 https://doi.org/10.1016/j.tibs.2010.05.009

Hinnebusch AG (2005) **Translational regulation of gcn4 and the general amino acid control of yeast** *Annu Rev Microbiol* 59: 407-450 https://doi.org/10.1146/annurev.micro.59.031805.133833

Hinnebusch AG, Ivanov IP, Sonenberg N (2016) **Translational control by 5'-untranslated regions of eukaryotic mrnas** *Science* 352: 1413-1416 https://doi.org/10.1126/science.aad9868

Hirschmann WD, Westendorf H, Mayer A, Cannarozzi G, Cramer P, Jansen RP (2014) **Scp160p is required for translational efficiency of codon-optimized mrnas in yeast** *Nucleic Acids Res* 42: 4043-4055 https://doi.org/10.1093/nar/gkt1392

Hogan DJ, Riordan DP, Gerber AP, Herschlag D, Brown PO (2008) **Diverse rna-binding proteins interact with functionally related sets of rnas, suggesting an extensive regulatory system** *PLoS Biol* 6: e255 https://doi.org/10.1371/journal.pbio.0060255

Inglis AJ, Masson GR, Shao S, Perisic O, McLaughlin SH, Hegde RS, Williams RL (2019) **Activation of gcn2 by the ribosomal p-stalk** *Proc Natl Acad Sci U S A* 116: 4946-4954 https://doi.org/10.1073/pnas.1813352116

Jackson RJ, Hellen CU, Pestova TV (2010) **The mechanism of eukaryotic translation initiation and principles of its regulation** *Nat Rev Mol Cell Biol* 11: 113-127 https://doi.org/10.1038/nrm2838

Jakovljevic J, Ohmayer U, Gamalinda M, Talkish J, Alexander L, Linnemann J, Milkereit P, Woolford JL, Jr. (2012) **Ribosomal proteins l7 and l8 function in concert with six a(3) assembly factors to propagate assembly of domains i and ii of 25s rrna in yeast 60s ribosomal subunits** *RNA* 18: 1805-1822 https://doi.org/10.1261/rna.032540.112

Jeffery CJ, Barry T, Doonan S, Petsko GA, Ringe D (1998) **Crystal structure of saccharomyces cerevisiae cytosolic aspartate aminotransferase** *Protein Sci* 7: 1380-1387 https://doi.org/10.1002/pro.5560070614

Kashiwagi K, Yokoyama T, Nishimoto M, Takahashi M, Sakamoto A, Yonemochi M, Shirouzu M, Ito T (2019) **Structural basis for eif2b inhibition in integrated stress response** *Science* 364: 495-499 https://doi.org/10.1126/science.aaw4104

Kershaw CJ, Costello JL, Castelli LM, Talavera D, Rowe W, Sims PF, Ashe MP, Hubbard SJ, Pavitt GD, Grant CM (2015) **The yeast la related protein slf1p is a key activator of translation during the oxidative stress response** *PLoS Genet* 11: e1004903 https://doi.org/10.1371/journal.pgen.1004903

Lee SJ, Swanson MJ, Sattlegger E (2015) **Gcn1 contacts the small ribosomal protein rps10, which is required for full activation of the protein kinase gcn2** *Biochem J* 466: 547-559 https://doi.org/10.1042/BJ20140782

Li AM, Vargas CA, Brykailo MA, Openo KK, Corbett AH, Fridovich-Keil JL (2004) **Both kh and non-kh domain sequences are required for polyribosome association of scp160p in yeast** *Nucleic Acids Res* 32: 4768-4775 https://doi.org/10.1093/nar/gkh812

Marton MJ, Vazquez de Aldana CR, Qiu H, Chakraburtty K, Hinnebusch AG (1997) **Evidence that gcn1 and gcn20, translational regulators of gcn4, function on elongating ribosomes in activation of eif2alpha kinase gcn2** *Mol Cell Biol* 17: 4474-4489 https://doi.org/10.1128/MCB.17.8.4474

Matia-Gonzalez AM, Laing EE, Gerber AP (2015) **Conserved mrna-binding proteomes in eukaryotic organisms** *Nat Struct Mol Biol* 22: 1027-1033 https://doi.org/10.1038/nsmb.3128

Matsuo Y, Ikeuchi K, Saeki Y, Iwasaki S, Schmidt C, Udagawa T, Sato F, Tsuchiya H, Becker T, Tanaka K, Ingolia NT, Beckmann R, Inada T (2017) **Ubiquitination of stalled ribosome triggers ribosome-associated quality control** *Nat Commun* 8: 159 https://doi.org/10.1038/s41467-017-00188-1

Merrick WC, Pavitt GD (2018) **Protein synthesis initiation in eukaryotic cells** *Cold Spring Harb Perspect Biol* 10 https://doi.org/10.1101/cshperspect.a033092

Meydan S, Guydosh NR (2020) **Disome and trisome profiling reveal genome-wide targets of ribosome quality control** *Mol Cell* 79: 588-602 e586 https://doi.org/10.1016/j.molcel.2020.06.010

Mills EW, Green R (2017) **Ribosomopathies: There's strength in numbers** *Science* 358 https://doi.org/10.1126/science.aan2755

Mitchell SF, Jain S, She M, Parker R (2013) **Global analysis of yeast mrnps** *Nat Struct Mol Biol* 20: 127-133 https://doi.org/10.1038/nsmb.2468

Morano KA, Grant CM, Moye-Rowley WS (2012) **The response to heat shock and oxidative stress in saccharomyces cerevisiae** *Genetics* 190: 1157-1195 https://doi.org/10.1534/genetics.111.128033

Pakos-Zebrucka K, Koryga I, Mnich K, Ljujic M, Samali A, Gorman AM (2016) **The integrated stress response** *EMBO Rep* 17: 1374-1395 https://doi.org/10.15252/embr.201642195

Palumbo RJ, Fuchs G, Lutz S, Curcio MJ (2017) **Paralog-specific functions of rpl7a and rpl7b mediated by ribosomal protein or snorna dosage in saccharomyces cerevisiae** *G3 (Bethesda)* 7: 591-606 https://doi.org/10.1534/g3.116.035931

Pavitt GD (2018) **Regulation of translation initiation factor eif2b at the hub of the integrated stress response** *Wiley Interdiscip Rev RNA* 9: e1491 https://doi.org/10.1002/wrna.1491

Perez-Riverol Y, Csordas A, Bai J, Bernal-Llinares M, Hewapathirana S, Kundu DJ, Inuganti A, Griss J, Mayer G, Eisenacher M, Perez E, Uszkoreit J, Pfeuffer J, Sachsenberg T, Yilmaz S, Tiwary S, Cox J, Audain E, Walzer M, Jarnuczak AF, Ternent T, Brazma A, Vizcaino JA (2019) **The pride database and related tools and resources in 2019: Improving support for quantification data** *Nucleic Acids Res* 47: D442-D450 https://doi.org/10.1093/nar/gky1106

Pochopien AA, Beckert B, Kasvandik S, Berninghausen O, Beckmann R, Tenson T, Wilson DN (2021) **Structure of gcn1 bound to stalled and colliding 80s ribosomes** *Proc Natl Acad Sci U S A* 118 https://doi.org/10.1073/pnas.2022756118

R Core Team (2019) **R: A language and environment for statistical computing**, https://www.r-project.org/.

Ramirez M, Wek RC, Hinnebusch AG (1991) **Ribosome association of gcn2 protein kinase, a translational activator of the gcn4 gene of saccharomyces cerevisiae** *Mol Cell Biol* 11: 3027-3036 https://doi.org/10.1128/mcb.11.6.3027-3036.1991

Richter JD (2007) **Cpeb: A life in translation** *Trends Biochem Sci* 32: 279-285 https://doi.org/10.1016/j.tibs.2007.04.004

Schuller AP, Wu CC, Dever TE, Buskirk AR, Green R (2017) **Eif5a functions globally in translation elongation and termination** *Mol Cell* 66: 194-205 e195 https://doi.org/10.1016/j.molcel.2017.03.003

Segev N, Gerst JE (2018) **Specialized ribosomes and specific ribosomal protein paralogs control translation of mitochondrial proteins** *J Cell Biol* 217: 117-126 https://doi.org/10.1083/jcb.201706059

Sen ND, Zhou F, Ingolia NT, Hinnebusch AG (2015) **Genome-wide analysis of translational efficiency reveals distinct but overlapping functions of yeast dead-box rna helicases ded1 and eif4a** *Genome Res* 25: 1196-1205 https://doi.org/10.1101/gr.191601.115

Shenton D, Smirnova JB, Selley JN, Carroll K, Hubbard SJ, Pavitt GD, Ashe MP, Grant CM (2006) **Global translational responses to oxidative stress impact upon multiple levels of protein synthesis** *J Biol Chem* 281: 29011-29021

Shiber A, Doring K, Friedrich U, Klann K, Merker D, Zedan M, Tippmann F, Kramer G, Bukau B (2018) **Cotranslational assembly of protein complexes in eukaryotes revealed by ribosome profiling** *Nature* 561: 268-272 https://doi.org/10.1038/s41586-018-0462-y

Slavov N, Semrau S, Airoldi E, Budnik B, van Oudenaarden A (2015) **Differential stoichiometry among core ribosomal proteins** *Cell Rep* 13: 865-873 https://doi.org/10.1016/j.celrep.2015.09.056

Swaney DL, Beltrao P, Starita L, Guo A, Rush J, Fields S, Krogan NJ, Villen J (2013) **Global analysis of phosphorylation and ubiquitylation cross-talk in protein degradation** *Nat Methods* 10: 676-682 https://doi.org/10.1038/nmeth.2519

Tesina P, Lessen LN, Buschauer R, Cheng J, Wu CC, Berninghausen O, Buskirk AR, Becker T, Beckmann R, Green R (2020) **Molecular mechanism of translational stalling by inhibitory codon combinations and poly(a) tracts** *EMBO J* 39: e103365 https://doi.org/10.15252/embj.2019103365

Tyanova S, Temu T, Cox J (2016) **The maxquant computational platform for mass spectrometry-based shotgun proteomics** *Nat Protoc* 11: 2301-2319 https://doi.org/10.1038/nprot.2016.136

Wang J, Zhou J, Yang Q, Grayhack EJ (2018) **Multi-protein bridging factor 1(mbf1), rps3 and asc1 prevent stalled ribosomes from frameshifting** *Elife* 7 https://doi.org/10.7554/eLife.39637

878 Wek RC (2018) **Role of eif2alpha kinases in translational control and adaptation to**
879 **cellular stress** *Cold Spring Harb Perspect Biol* 10
880 https://doi.org/10.1101/cshperspect.a032870
881 Winefield CS, Farnden KJ, Reynolds PH, Marshall CJ (1995) **Evolutionary analysis of**
882 **aspartate aminotransferases** *J Mol Evol* 40: 455-463
883 https://doi.org/10.1007/BF00164031
884 Woolford JL, Jr., Baserga SJ (2013) **Ribosome biogenesis in the yeast saccharomyces**
885 **cerevisiae** *Genetics* 195: 643-681 https://doi.org/10.1534/genetics.113.153197
886 Wu CC, Peterson A, Zinshteyn B, Regot S, Green R (2020) **Ribosome collisions trigger**
887 **general stress responses to regulate cell fate** *Cell* 182: 404-416 e414
888 https://doi.org/10.1016/j.cell.2020.06.006
889 Wu CC, Zinshteyn B, Wehner KA, Green R (2019) **High-resolution ribosome profiling**
890 **defines discrete ribosome elongation states and translational regulation during**
891 **cellular stress** *Mol Cell* 73: 959-970 e955
892 https://doi.org/10.1016/j.molcel.2018.12.009
893 Yan LL, Zaher HS (2021) **Ribosome quality control antagonizes the activation of the**
894 **integrated stress response on colliding ribosomes** *Mol Cell* 81: 614-628 e614
895 https://doi.org/10.1016/j.molcel.2020.11.033
896 Yourik P, Aitken CE, Zhou F, Gupta N, Hinnebusch AG, Lorsch JR (2017) **Yeast eif4a**
897 **enhances recruitment of mrnas regardless of their structural complexity** *Elife* 6
898 https://doi.org/10.7554/eLife.31476
899 Yu CH, Dang Y, Zhou Z, Wu C, Zhao F, Sachs MS, Liu Y (2015) **Codon usage influences**
900 **the local rate of translation elongation to regulate co-translational protein**
901 **folding** *Mol Cell* 59: 744-754 https://doi.org/10.1016/j.molcel.2015.07.018
902

Figures and Legends

Figure 1

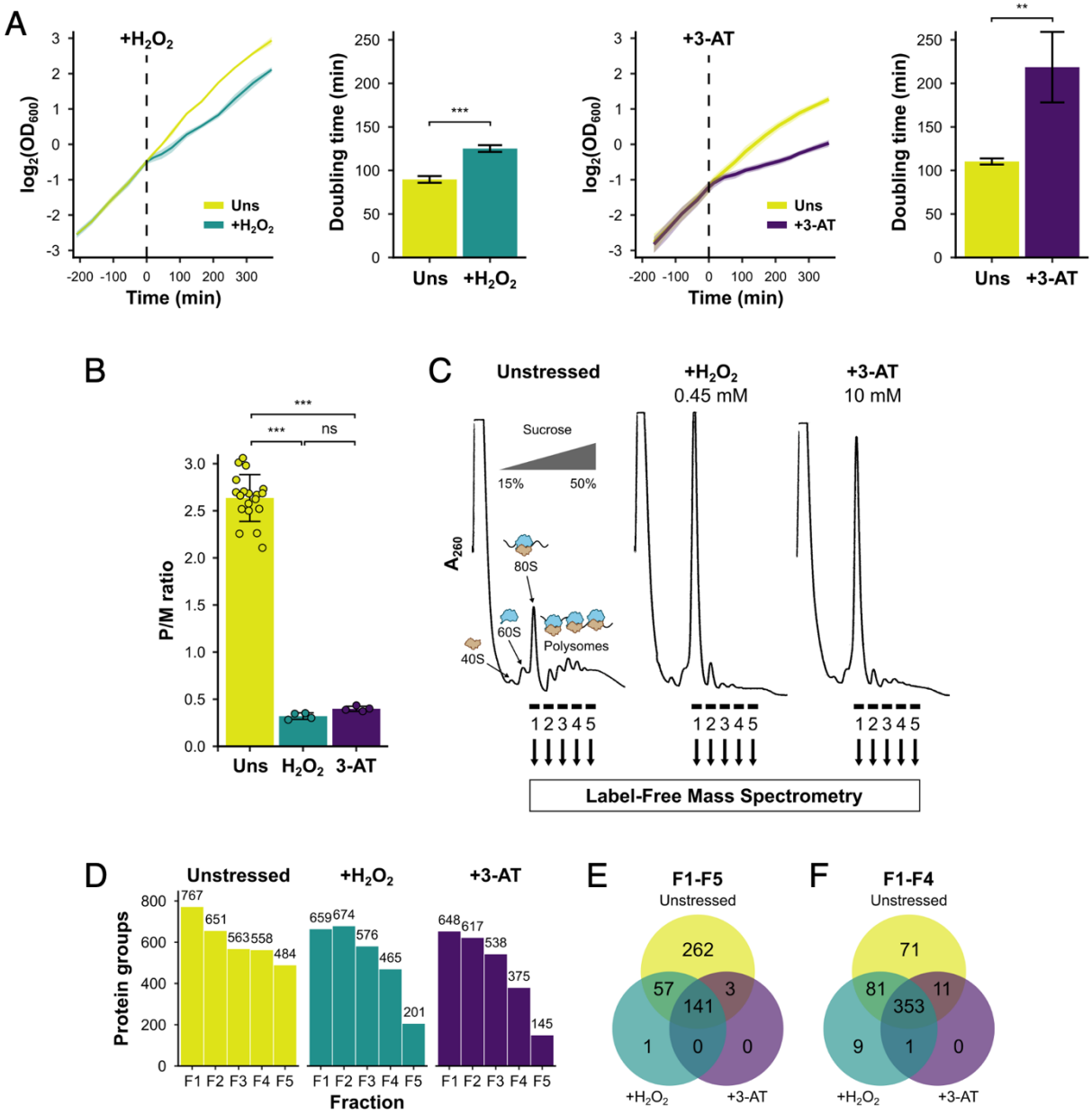

Figure 1. Identification of translational regulators using polysomal proteomics

(A) Growth curves and doubling times for unstressed, 0.45 mM H_2O_2-treated and 10 mM 3-AT-treated cultures (n=3). The time of H_2O_2 or 3-AT addition is indicated. (B) Quantification of polysome-to-monosome (P/M) ratios under the three conditions (n=4-19). Error bars show standard deviation (SD). The t-test was used to compare the conditions: ns – not significant ($p > 0.05$), * – $p < 0.05$, ** – $p < 0.01$, *** – $p < 0.001$. (C) Overview of polysomal proteomics. Monosomal (F1) and polysomal (F2-F5) fractions were isolated from unstressed, H_2O_2-treated and 3-AT-treated extracts and analysed using label-free MS. (D) The number of proteins identified reproducibly (≥ 2 replicates) in each fraction. (E-F) Venn-style diagrams of overlaps between conditions for proteins found across (E) all five fractions or (F) the first four fractions.

Figure 1–figure supplement 1

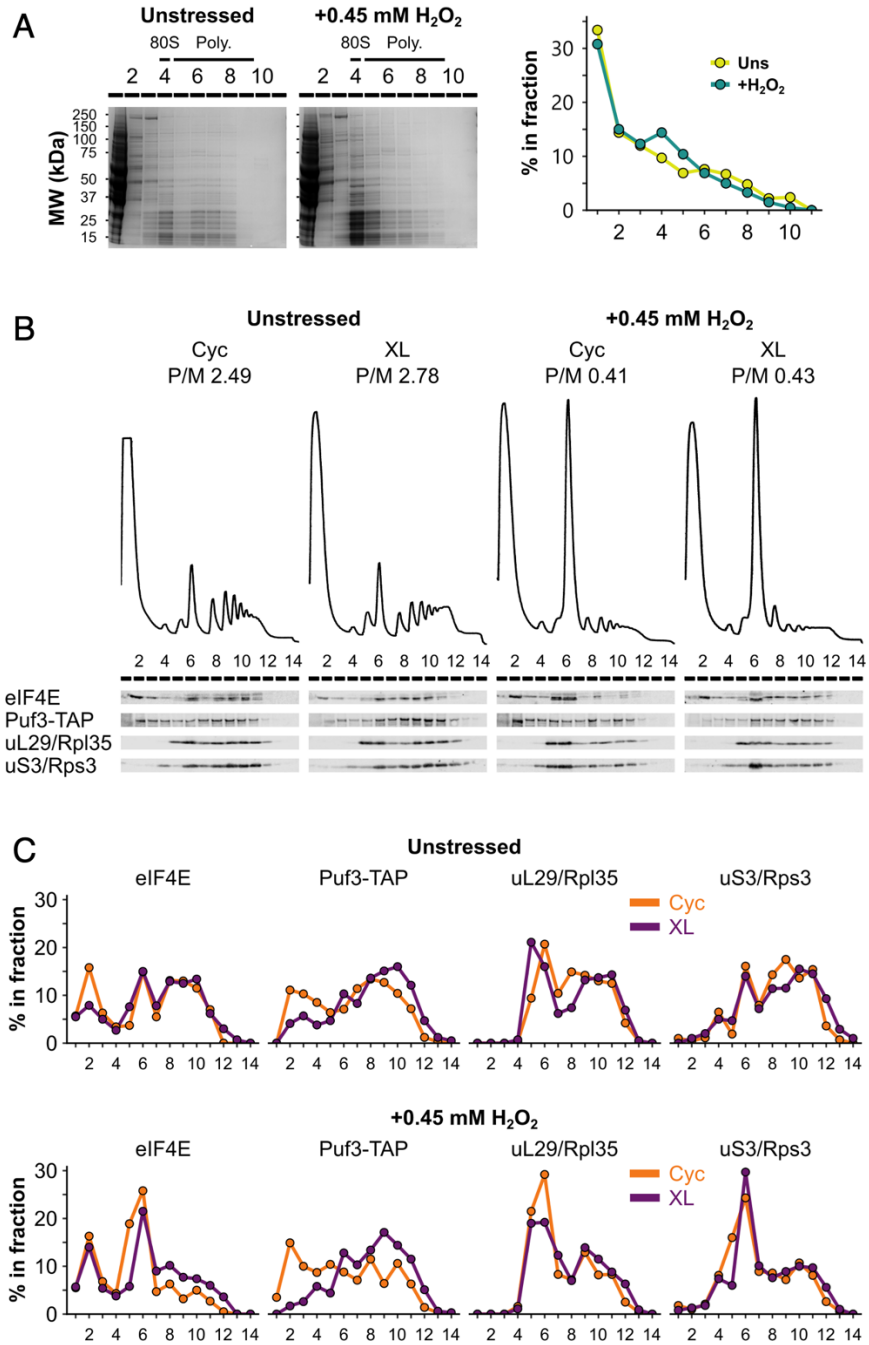

Figure 1–figure supplement 1. Formaldehyde crosslinking prevents ribosome run-off and retains RBPs in polysome fractions similarly to cycloheximide treatment

(A) Left: SDS-PAGE analysis of fractions from unstressed and H_2O_2-treated extracts run on 15-50% sucrose gradients. Right: quantification of entire lanes using LI-COR Image Studio. (B) Polysome profiles and western blots comparing cycloheximide treatment (Cyc) and formaldehyde crosslinking (XL) of cultures for preparing extracts for polysome profiling. (C) Bands from (B) were quantified using LI-COR Image Studio and the proportion of each protein in each fraction was calculated.

Figure 1–figure supplement 2

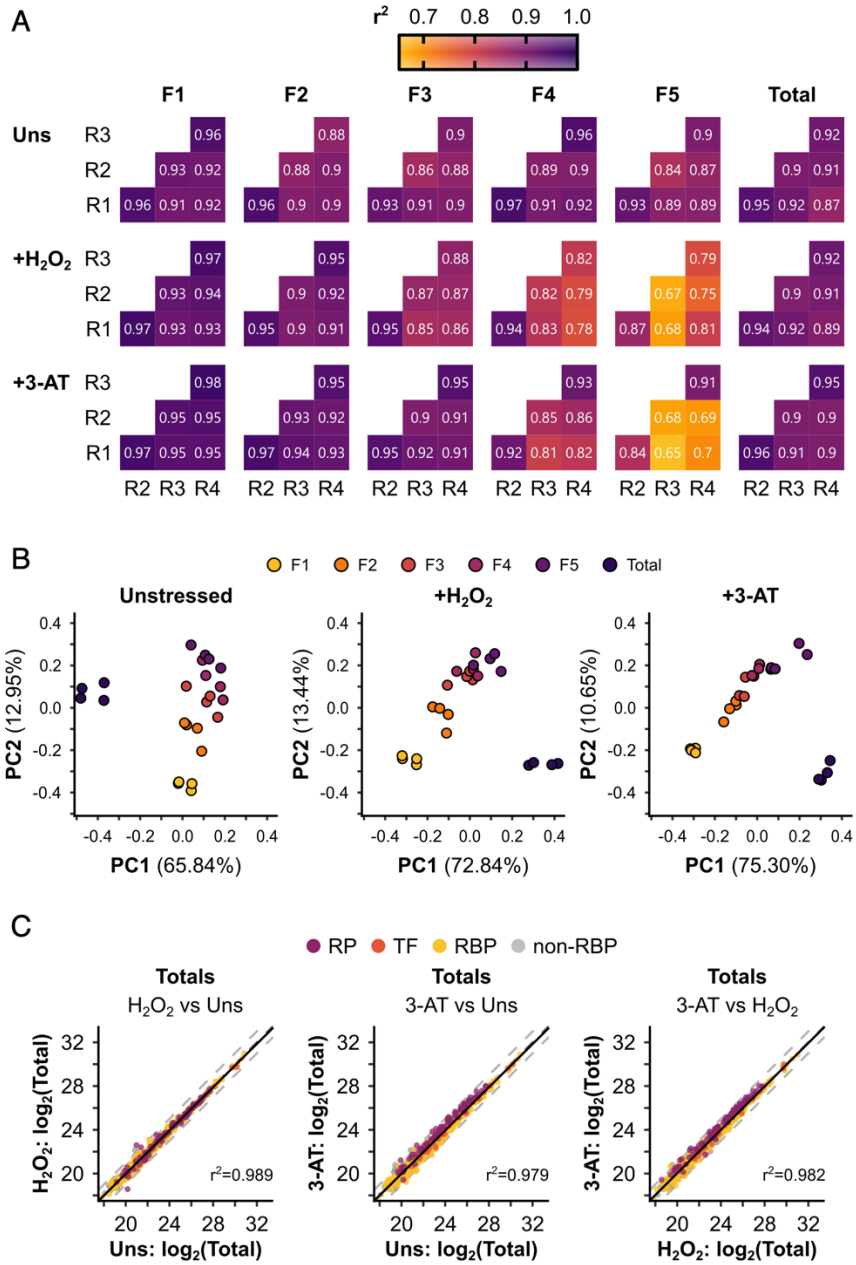

Figure 1–figure supplement 2. Polysomal proteomics data are reproducible and can separate the different fractions

(A) r^2 values for pairwise correlations between replicates (R1-R4) for each sample. (B) Principle component analysis (PCA) of the different samples under each condition. The percentage of the variation explained by each of the first two principle components is indicated. The axes are not equivalent for the different conditions. Note that only protein groups present in all of the samples for a given condition could be included in the comparison. (C) Pairwise comparisons between conditions for the totals. r^2 values from linear regressions are indicated. Protein groups are coloured by their functional category: RP – ribosomal protein, TF – translation factor, RBP – RNA-binding protein, non-RBP – other protein.

Figure 1–figure supplement 3

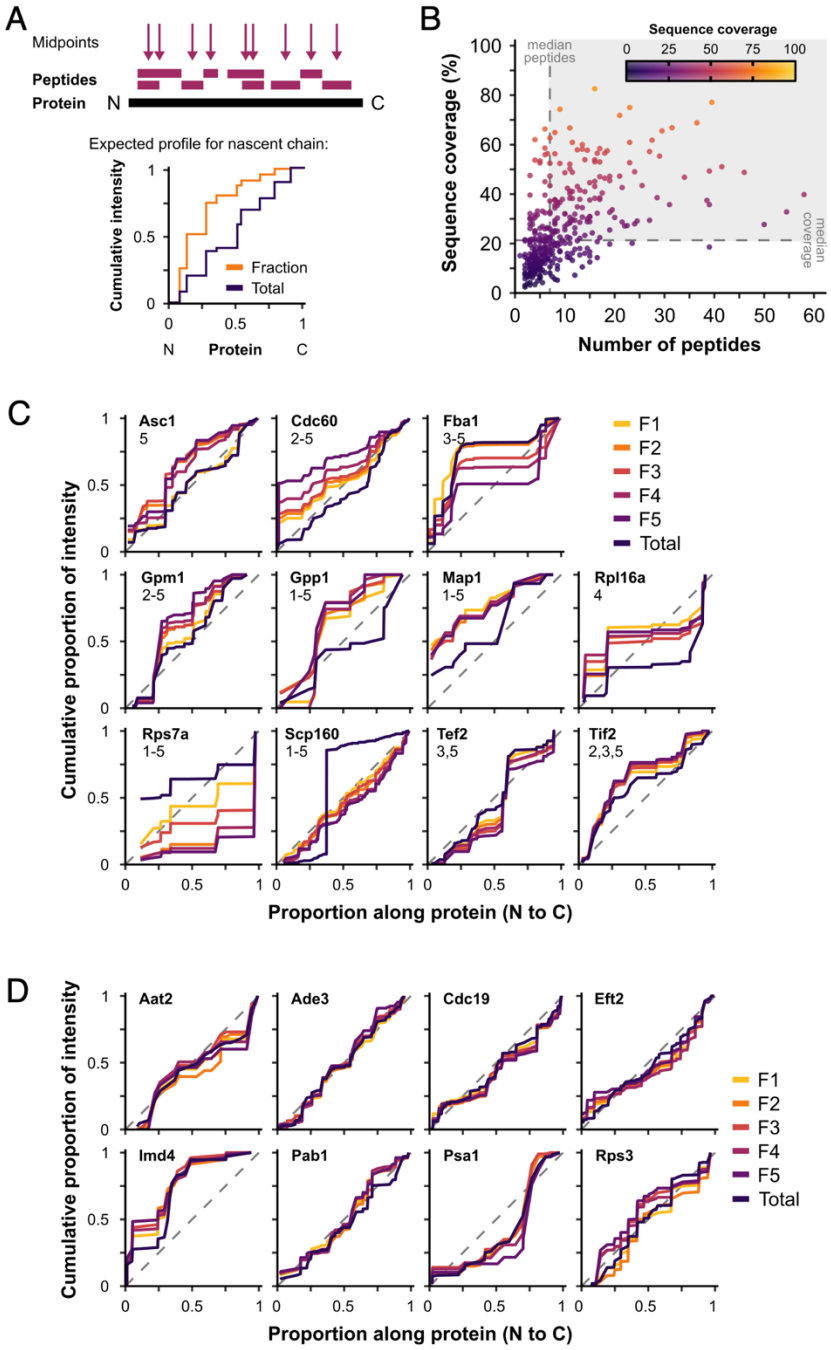

Figure 1–figure supplement 3. Nascent peptides are not a major contributor to protein signal

We hypothesised that proteins represented in polysome fractions by nascent chains and/or co-translational complex formation would show greater intensity from N-terminal peptides in F1-F5 than in totals, as they are synthesised in the N-to-C direction. (A) Peptide midpoint calculation and example cumulative peptide intensity distribution. Steps in the cumulative intensity profiles indicate peptide midpoints. For a protein detected in polysome fractions (Fraction) through only nascent chains, a shift in signal accumulation compared with a

944 cytoplasmic extract (Total) would be expected, such that a much greater proportion of the total
945 peptide intensity would be expected from the N-terminal end of the protein. (B) Median number
946 of peptides and median sequence coverage (percentage of the amino acid residues that were
947 detected by MS in at least one peptide) for individual proteins in unstressed samples (371
948 uniquely detected proteins). Proteins in the shaded area were used for the analysis (142
949 proteins). (C-D) Cumulative peptide intensity distributions for fractions and totals of named
950 proteins. Differences between fractions and totals were tested using the Kolmogorov-Smirnov
951 test. (C) The proteins with significantly different fraction distributions compared with totals (p
952 < 0.05). The fractions that are significantly different are indicated by number. Only 6 of 142
953 showed some evidence of a bias towards the N-terminus in one or more fractions (Asc1,
954 Cdc60, Gpm1, Gpp1, Map1 and eIF4A/Tif2), while 5 others (Fba1, Rpl16a, Rps7a, Scp160
955 and eEF1A/Tef2) showed different patterns. (D) Representative examples of proteins without
956 significant differences between fractions and totals. Dashed lines are y=x.
957
958

Figure 2

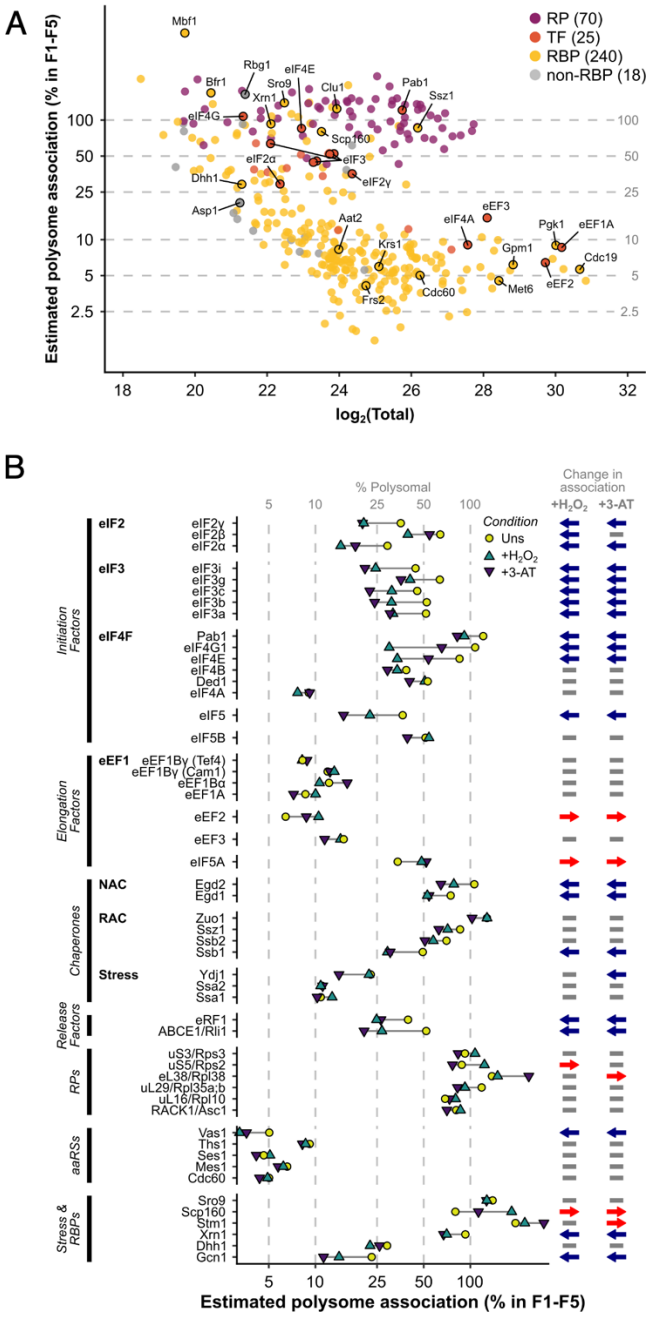

Figure 2. The ribosome association of initiation factors decreases during stress

(A) Ribosome association of proteins in F1-F4 under all three conditions (353 proteins). The proportion of each protein that is ribosome-associated (% polysomal) was estimated by comparing the summed intensity in the fractions with the totals (see Methods). Protein groups are coloured by their functional category: RP – ribosomal protein, TF – translation factor, RBP – RNA-binding protein, non-RBP – other protein. The number of proteins in each functional category is indicated. (B) The change in overall ribosome association during both stresses for selected translation-related proteins. The direction of the change (if any) in ribosome association is indicated: blue arrow – decrease, red arrow – increase.

Figure 3

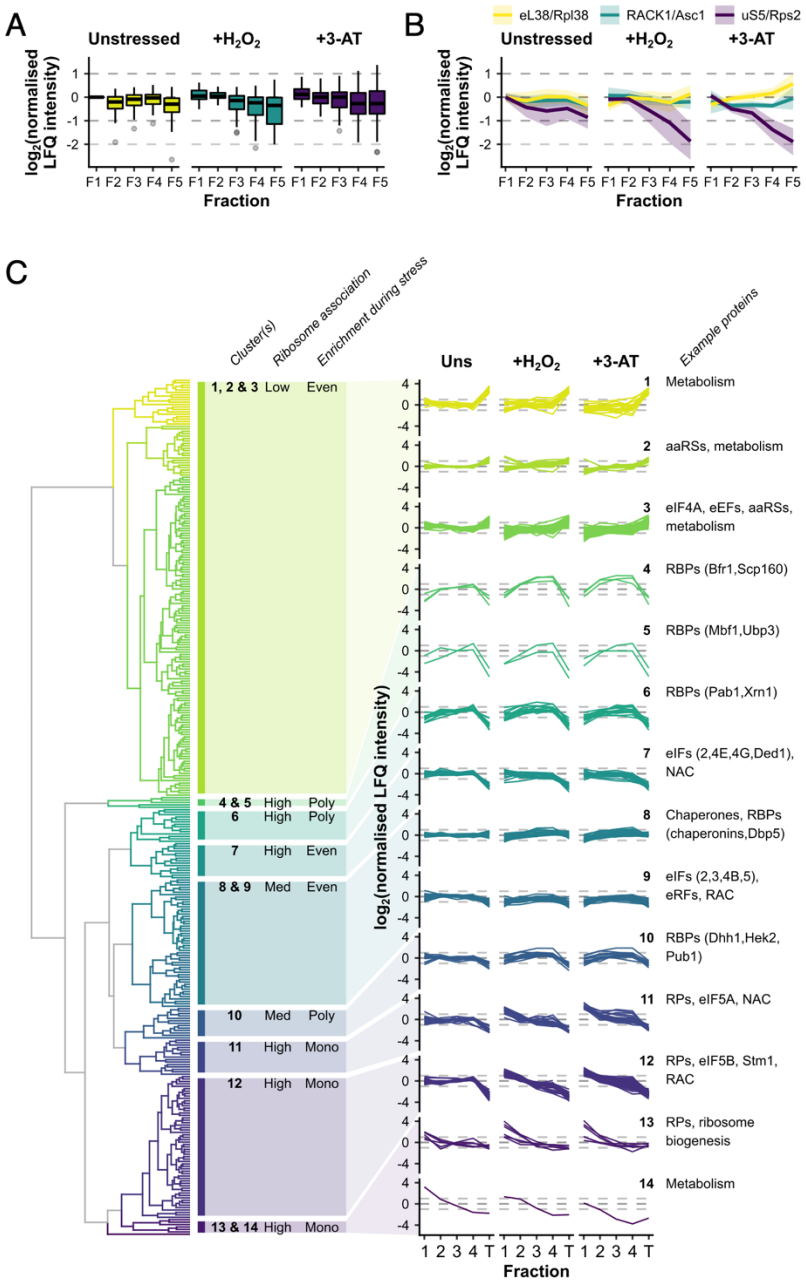

Figure 3. RPs and RBPs show distinct patterns of polysome enrichment

(A) The LFQ intensities for each RP identified in all conditions F1-F5 were normalised to Rps3/uS3 on a fraction-by-fraction basis and then to unstressed F1. Boxplots showing the distribution of normalised LFQ intensities in each sample. (B) Polysome association profiles for three example RPs normalised to Rps3/uS3. Shaded areas show mean ±SD. (C) Clustered 'polysome enrichment profiles' for proteins identified under all three conditions in F1-F4. The LFQ intensities for each protein were normalised only to its own mean across the unstressed fractions. T – total. The overall ribosome association and PE during stress for each cluster or group of clusters is indicated: Poly – polysome-enriched, Mono – monosome-enriched, Even – equally enriched in all fractions.

Figure 3–figure supplement 1

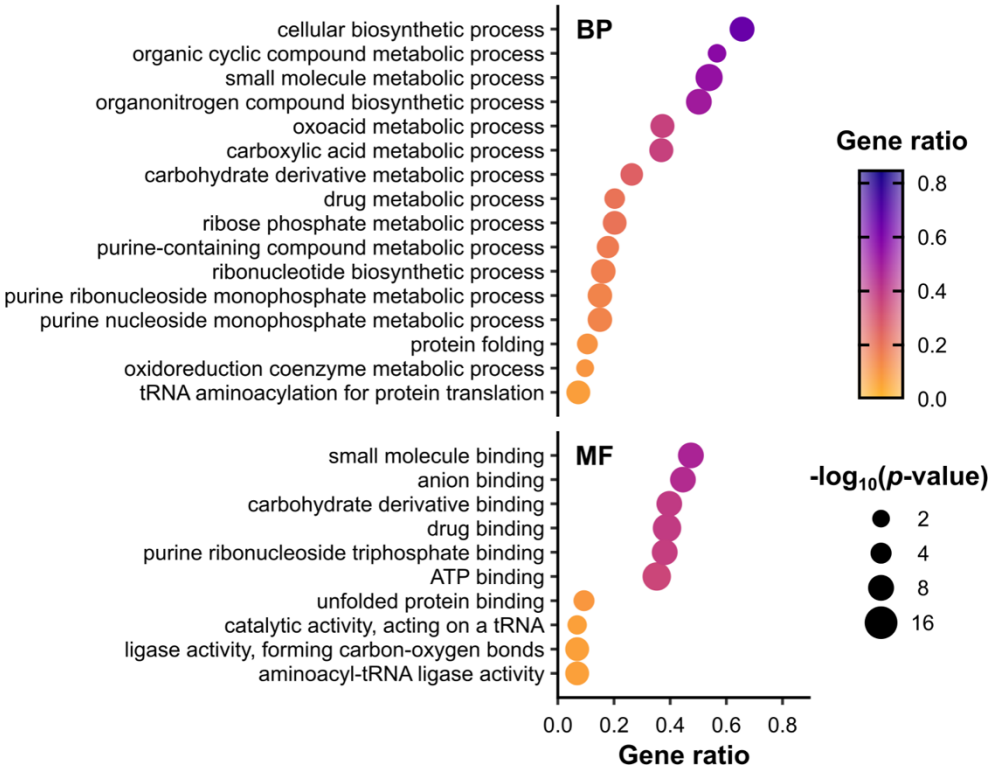

Figure 3–figure supplement 1. Metabolic functions are enriched among RBPs identified in polysomal fractions

Overrepresentation analysis of gene ontology (GO) terms associated with proteins in all conditions F1-F4, performed using the R package *clusterProfiler* (Yu et al, 2012). *p*-values were calculated using Fisher's exact test, with false discovery rate (FDR) correction for multiple testing. The set of all proteins identified in at least one MS sample was used as the background (Supplementary file 1–sheet 1). To focus on RBPs and other proteins, RPs and translation factors were also excluded from both the test set and the background set. Only enriched terms with *p*-value ≤ 0.01 ($-\log_{10}$(adjusted *p*-value) ≥ 2) are shown. Gene ratio is the proportion of the test set annotated with a given GO term. BP – biological process, MF – molecular function. No cellular component (CC) terms were significantly enriched in this set. See Supplementary file 1–sheet 4 for the full list of proteins associated with each term.

Figure 4

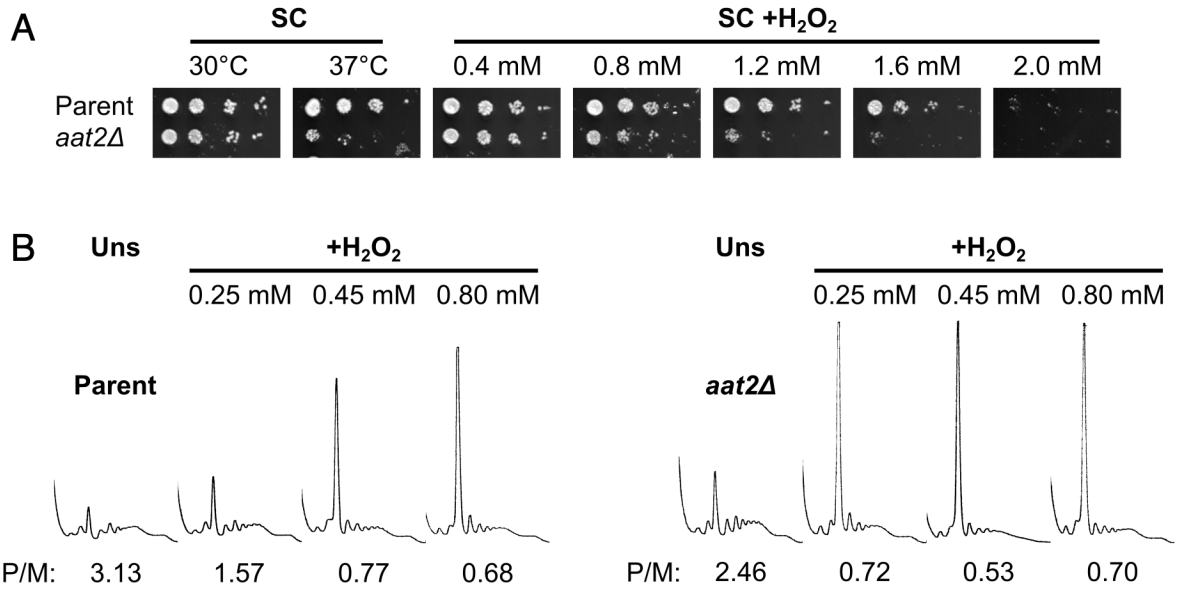

Figure 4. Deletion of *AAT2* increases oxidative stress sensitivity

(A) Spotting assay on synthetic complete dextrose (SC) medium in the presence of varying concentrations of H_2O_2. Each spot is a 10-fold dilution of the previous one. (B) Representative polysome profiles from unstressed (B) and H_2O_2-treated (C) cultures. P/M: mean polysome-to-monosome ratio (n=2-3).

Figure 4–figure supplement 1

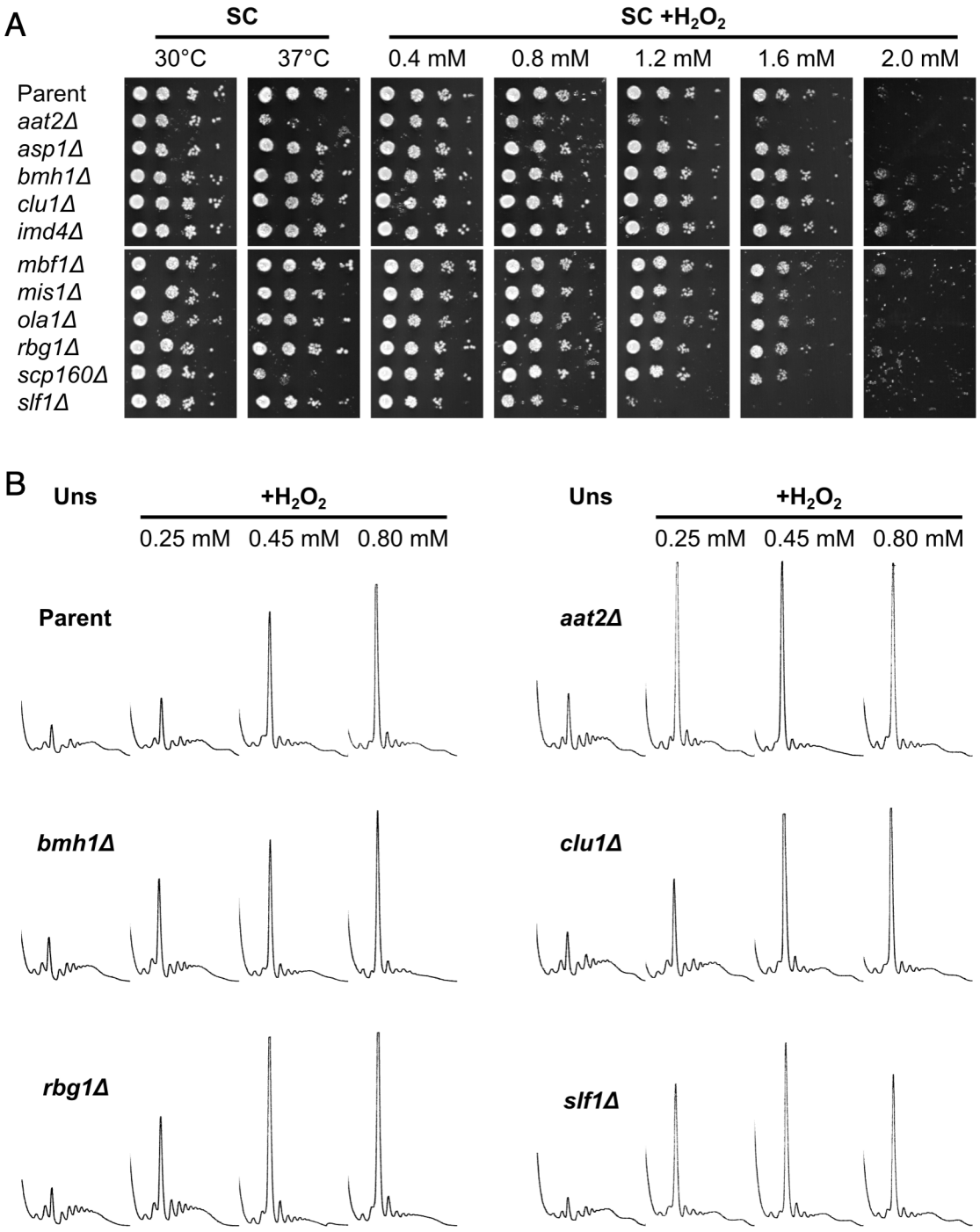

Figure 4–figure supplement 1. Deletion of *AAT2* increases oxidative stress sensitivity

Deletion strains for multiple candidate RBPs identified by polysomal proteomics were tested for sensitivity to oxidative stress. The *slf1Δ* strain was previously observed to be hypersensitive to oxidative stress so was used as a control (Kershaw et al. 2015). (A) Spotting assay on synthetic complete dextrose (SC) medium in the presence of varying concentrations of H_2O_2. Each spot is a 10-fold dilution of the previous one. (B) Representative polysome profiles from unstressed and H_2O_2-treated cultures (n=2-3).

Figure 5

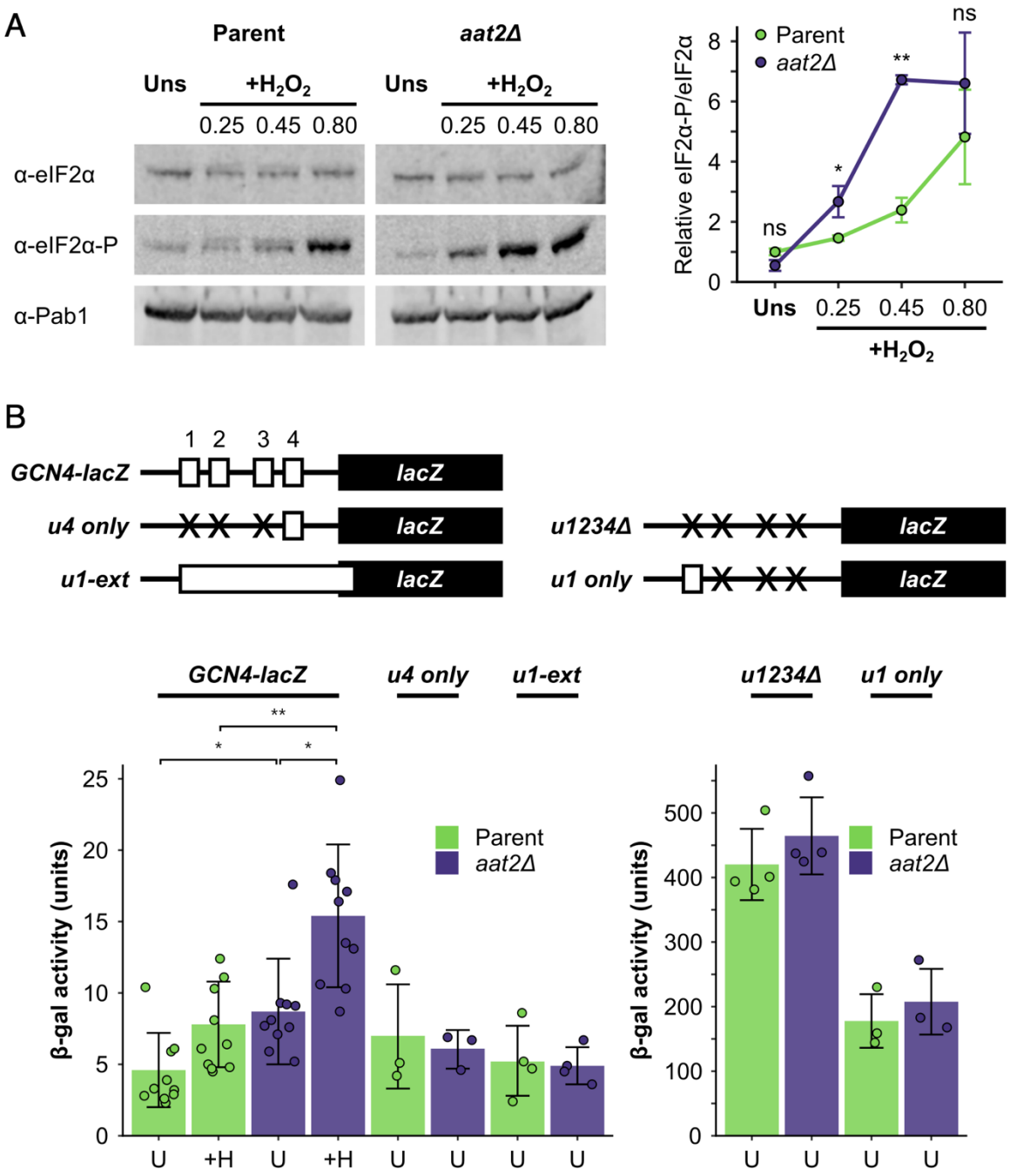

Figure 5. Deletion of *AAT2* enhances Gcn2 activity during oxidative stress

(A) Left: representative western blots showing eIF2α phosphorylation in unstressed and H_2O_2-treated cultures. Right: bands were quantified using LI-COR Image Studio and the eIF2α-P/eIF2α ratio was calculated. Error bars show SD (n=3). (B) Top: *GCN4-lacZ* reporter constructs used to test the translational activation of *GCN4*. Solid boxes – *lacZ* ORF, open boxes – *GCN4* upstream ORFs, crosses – removed *GCN4* uORFs. Bottom: β-galactosidase activity in strains transformed with *GCN4-lacZ* reporter plasmids (n=3-10). Error bars show SD. U – unstressed. +H – +0.45 mM H_2O_2. The t-test was used to compare the strains: ns – not significant ($p > 0.05$), * – $p < 0.05$, ** – $p < 0.01$, *** – $p < 0.001$.

Figure 6

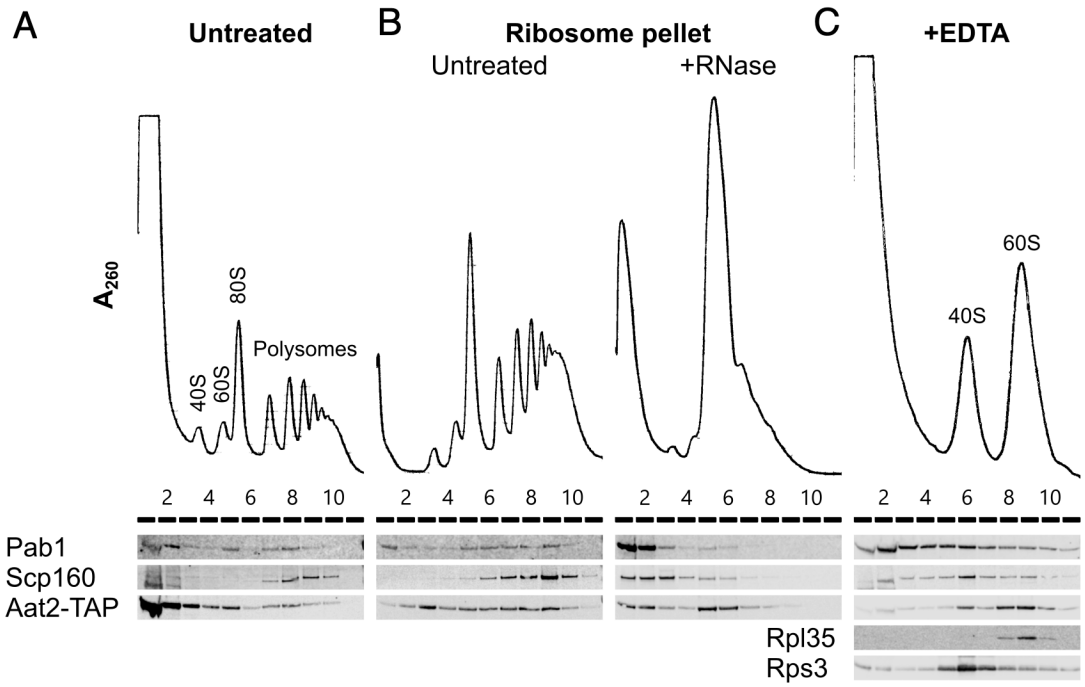

Figure 6: Aat2 binds to 60S ribosomes

(A) Representative polysome profile and western blot from an unstressed Aat2-TAP extract run on a 15-50% sucrose gradient. (B) Ribosome pellets from unstressed Aat2-TAP extracts were isolated using sucrose cushions, then either left untreated or treated with RNase I prior to polysome profiling. (C) Representative polysome profile and western blot from an unstressed Aat2-TAP extract treated with 50 mM EDTA and run on a 10-25% sucrose gradient to separate the ribosomal subunits.

Figure 7

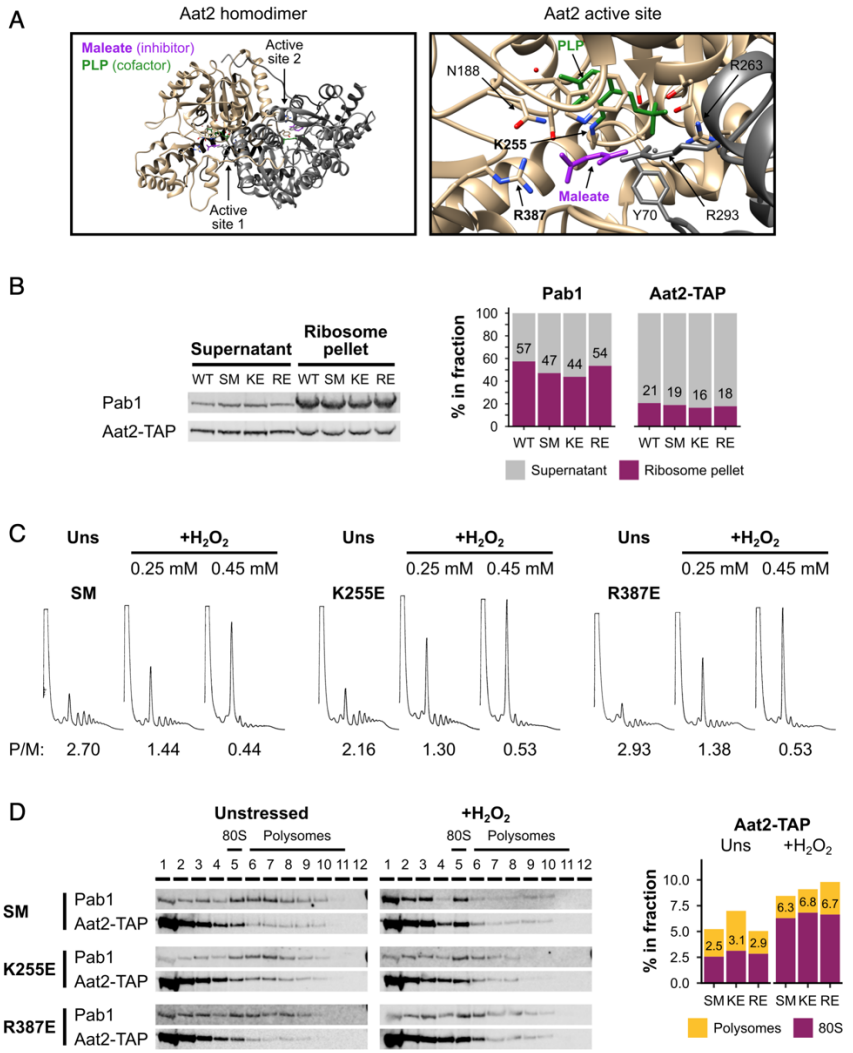

Figure 7: Non-catalytic mutants of Aat2 remain polysome-associated and do not show heightened stress sensitivity

(A) Views of the Aat2 homodimer (left) and active site (right), showing the cofactor pyridoxal-5'-phosphate (PLP, green) and the competitive inhibitor maleate (purple; PDB 1YAA (Jeffery et al. 1998)). The two active site residues targeted by site-directed mutagenesis are in bold. (B) Left: ribosome pellets were separated from supernatants using sucrose cushions and analysed by western blotting. Right: bands were quantified using LI-COR Image Studio and the percentage of signal from each of the two fractions was calculated. Values are indicated for the ribosome pellet fraction. (C) Representative polysome profiles from unstressed and H_2O_2-treated cultures. P/M: mean polysome-to-monosome ratio (n=2-3). (D) Left: representative western blots of sucrose gradient fractions from mutated Aat2-TAP strains. The positions of the 80S/monosome and polysome fractions are indicated. Right: mean quantification of Aat2-TAP in the 80S and polysome fractions for each strain. Values are indicated for the 80S fraction. WT – Aat2-TAP parent strain, SM – control with silent mutations, KE/K255E – Aat2^{K255E}-TAP, RE/R387E – Aat2^{R387E}-TAP.

Figure 7–figure supplement 1

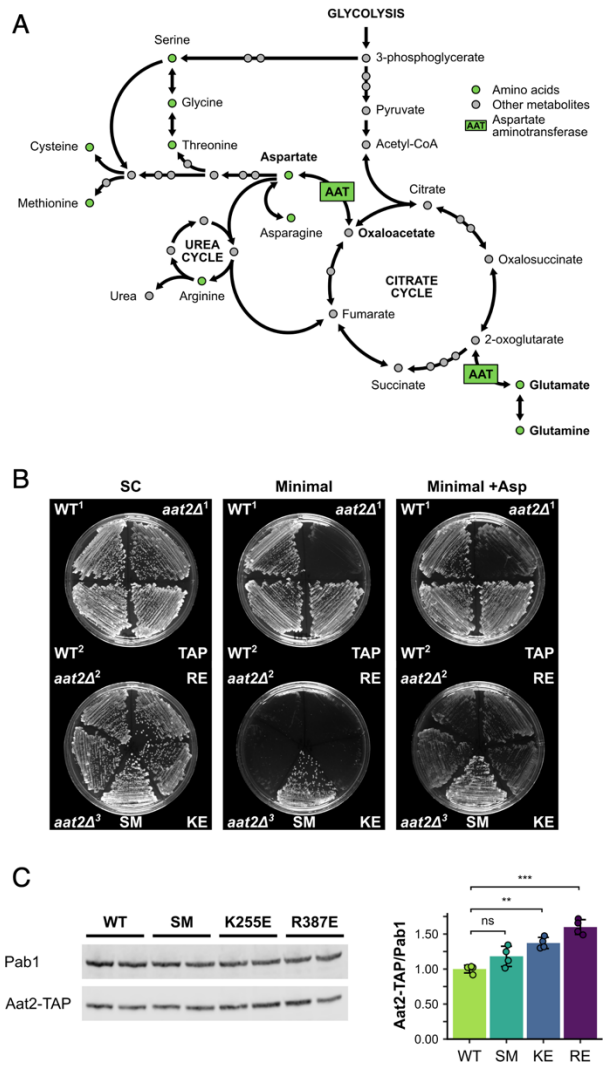

Figure 7–figure supplement 1. Non-catalytic *AAT2* mutants are auxotrophic for aspartate and well-expressed

(A) The role of aspartate aminotransferase (AAT) in linking the citrate cycle with amino acid biosynthesis. Both *AAT1* and *AAT2* encode AAT in *S. cerevisiae*. Its substrates are in bold. Other pathways are available for the interconversion of 2-oxoglutarate and glutamate. Adapted from KEGG (Ogata et al, 1999). For clarity, some links are not shown. (B) Growth of parent (WT and Aat2-TAP), deletion (*aat2Δ*) and *AAT2* mutant strains (SM – control with silent mutations, KE/K255E – Aat2^{K255E}-TAP, RE/R387E – Aat2^{R387E}-TAP) on SC, minimal medium and minimal medium supplemented with *L*-aspartate (+Asp). (C) Left: representative western blot of cell extracts from Aat2-TAP wild-type (WT) and mutant (SM, K255E and R387E) strains. Right: quantification of Aat2-TAP expression relative to Pab1 in the WT and mutant strains (n=4). Error bars show SD. The t-test was used to compare the strains: ns – not significant ($p > 0.05$), * – $p < 0.05$, ** – $p < 0.01$, *** – $p < 0.001$.

Figure 7–figure supplement 2

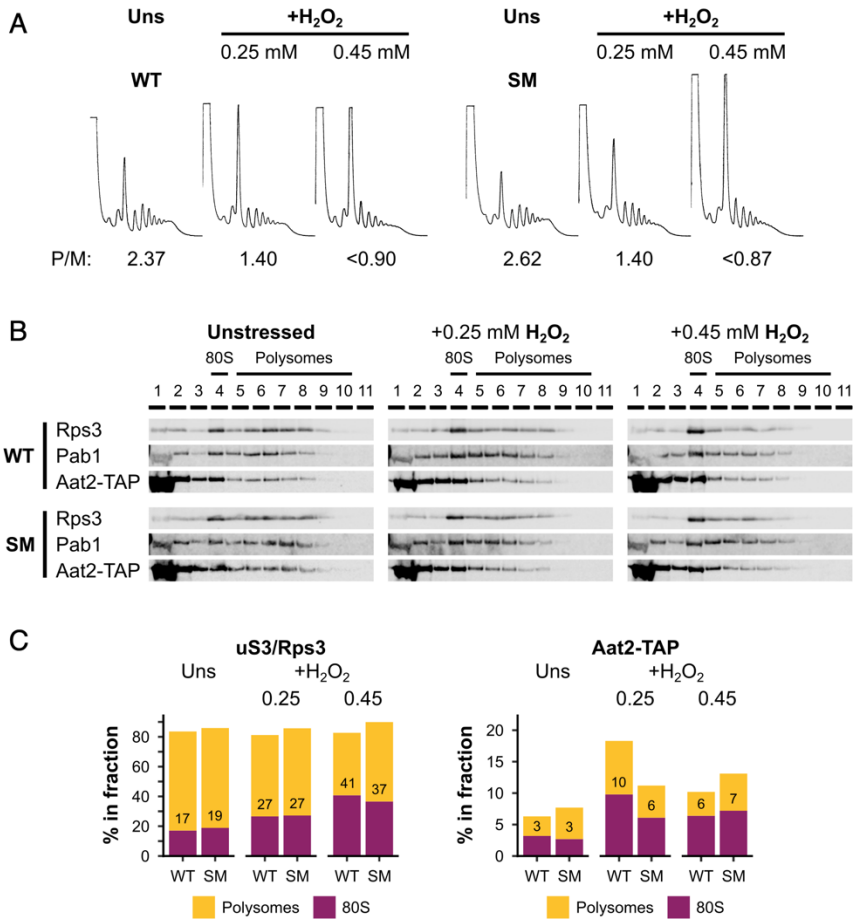

Figure 7–figure supplement 2. Silent mutations do not affect oxidative stress sensitivity or Aat2 polysome association

(A) Polysome profiles from unstressed and H_2O_2-treated cultures of the Aat2-TAP parent strain (WT) and Aat2^{SM}-TAP strains (SM; Aat2-TAP control with silent mutations). P/M – polysome-to-monosome ratio. (B) Western blots of sucrose gradient fractions from extracts of the WT and SM strains. The positions of the 80S/monosomes and polysomes are indicated. (C) Quantification of the 80S/monosomal and polysomal proportions of uS3/Rps3 and Aat2-TAP in the two strains under each condition. The monosomal proportion is indicated.